

UC Berkeley

UC Berkeley Previously Published Works

Title

MEMS technology for timing and frequency control

Permalink

<https://escholarship.org/uc/item/19m6207z>

Journal

IEEE Transactions on Ultrasonics Ferroelectrics and Frequency Control, 54(2)

ISSN

0885-3010

Author

Nguyen, CTC

Publication Date

2007-02-01

Peer reviewed

MEMS Technology for Timing and Frequency Control

Clark T.-C. Nguyen, *Fellow, IEEE*

Abstract—An overview on the use of microelectromechanical systems (MEMS) technologies for timing and frequency control is presented. In particular, micromechanical RF filters and reference oscillators based on recently demonstrated vibrating on-chip micromechanical resonators with Q 's $> 10,000$ at 1.5 GHz are described as an attractive solution to the increasing count of RF components (e.g., filters) expected to be needed by future multiband, multimode wireless devices. With Q 's this high in on-chip abundance, such devices might also enable a paradigm shift in the design of timing and frequency control functions, where the advantages of high- Q are emphasized, rather than suppressed (e.g., due to size and cost reasons), resulting in enhanced robustness and power savings. Indeed, as vibrating RF MEMS devices are perceived more as circuit building blocks than as stand-alone devices, and as the frequency processing circuits they enable become larger and more complex, the makings of an integrated micromechanical circuit technology begin to take shape, perhaps with a functional breadth not unlike that of integrated transistor circuits. With even more aggressive three-dimensional MEMS technologies, even higher on-chip Q 's are possible, such as already achieved via chip-scale atomic physics packages, which so far have achieved Q 's $> 10^7$ using atomic cells measuring only 10 mm^3 in volume and consuming just 5 mW of power, all while still allowing atomic clock Allan deviations down to 10^{-11} at one hour.

I. INTRODUCTION

THE performance of our electronic systems is generally limited by the accuracy and stability of the clocks or frequency references they use. For example, the ability and speed with which a global positioning system (GPS) receiver can lock to a GPS satellite's pseudorandom signal and obtain position is dependent heavily upon how well synchronized its internal clock is to that of the satellite; here, the better the internal clock, the more likely and faster the lock. Unfortunately, our best clocks and frequency references (e.g., atomic clocks, oven stabilized crystal oscillators) are often too large or consume too much power to be used in portable applications. This forces us to keep our best electronic systems on tabletops and out of the hands of users, who must then access them through

sometimes unreliable remote channels. Indeed, a technology capable of miniaturizing and lowering the power consumption of our best timekeepers and frequency references to the point of allowing insertion into truly portable applications would be most welcome.

Among the many applications enabled by timing and frequency control, portable wireless communications stand to benefit most from miniaturization technology, since an ability to shrink high- Q passives can potentially change the premises under which wireless subsystems are designed. In particular, today's wireless transceivers are designed under a near mandate to minimize or eliminate, inasmuch as possible, the use of high- Q passives. The reasons for this are quite simple: cost and size. Specifically, the ceramic filters, surface acoustic wave (SAW) filters, quartz crystals, and now film bulk acoustic resonator (FBAR) filters, capable of achieving the Q 's from 500–10,000 needed for RF and IF bandpass filtering and frequency generation functions, are all off-chip components that must interface with transistor functions at the board level, taking up a sizable amount of board space and comprising a sizable fraction of the parts and assembly cost.

Pursuant to reducing the off-chip parts count in modern cellular handsets, direct-conversion [1] or low-IF [2] receiver architectures have removed the IF filter, and integrated inductor technologies are removing some of the off-chip L 's used for bias and matching networks [3]. Although these methods can lower cost, they often do so at the expense of increased transistor circuit complexity and more stringent requirements on circuit performance (e.g., dynamic range), both of which degrade somewhat the robustness and power efficiency of the overall system. In addition, the removal of the IF filter does little to appease the impending needs of future multiband, multimode reconfigurable handsets that will likely require high- Q RF filters in even larger quantities—perhaps one set for each wireless standard to be addressed. Fig. 1 presents the simplified system block diagram for an example handset receiver targeted for multiband operation, clearly showing that it is the high- Q RF filters, not the IF filter, that must be addressed. In the face of this need, and without a path by which the RF filters can be removed, an option to reinsert high Q components without the size and cost penalties of the past would be most welcome, especially if done in a manner that allows co-integration of passives with transistors onto the same chip.

In this regard, microelectromechanical systems (MEMS) technology, with its ability to shrink mechanical features and mechanisms down to micron (and even nano) scales,

Manuscript received April 7, 2006; accepted August 23, 2006. Much of this work was supported by the Defense Advanced Research Projects Agency (DARPA) and the National Science Foundation (NSF).

C. T.-C. Nguyen was with the Department of Electrical Engineering and Computer Science, University of Michigan, Ann Arbor, MI 48109-2122. He is now with the Department of Electrical Engineering and Computer Science, University of California at Berkeley, Berkeley, CA 94720 (e-mail: ctnguyen@eecs.berkeley.edu).

Digital Object Identifier 10.1109/TUFFC.2007.240

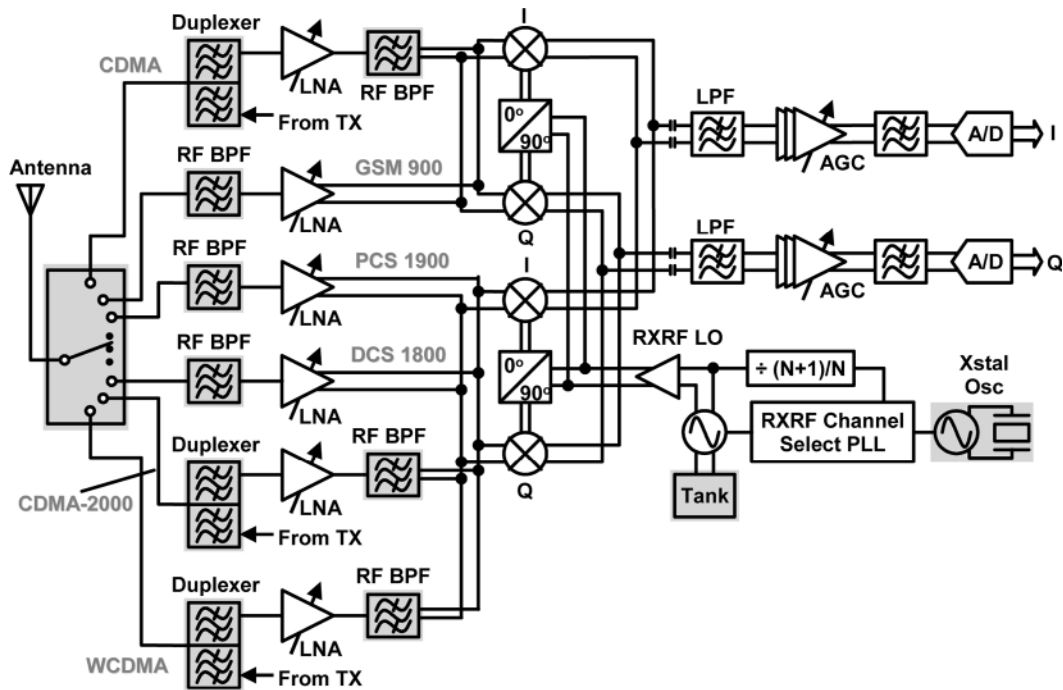


Fig. 1. System block diagram of a future multimode receiver front end, showing how the number of RF passives will continue to increase, regardless of whether or not a direct-conversion architecture is used.

already provides substantial size and power reduction for applications spanning displays, sensors, and fluidic systems, and is now emerging to provide similar advantages for timekeepers and frequency control functions in portable wireless devices [4], [5]. In particular, vibrating micromechanical resonator devices based on silicon micromachining technologies have now been demonstrated with on-chip Q 's greater than 10,000 at GHz frequencies [6], [7], frequency- Q products exceeding 2.75×10^{13} [6], temperature stability better than 18 ppm over 27 to 107°C [8], and aging stabilities better than 2 ppm over one year [9], [10]. They have also been embedded into oscillator circuits to achieve phase noise performance satisfying global systems for mobile communications (GSM) specifications for reference oscillators [11]–[13]. In addition, a combination of MEMS and microphotonic technologies have now achieved 10-cm³ complete atomic clocks consuming less than 200 mW of power, while still attaining Allan deviations better than 5×10^{-11} at 100 s. Continued scaling of such devices that take advantage of compressed control time constants and lower heating power consumption is expected to soon yield complete atomic clocks in less than 1 cm³ and consuming less than 30 mW of power, while still achieving an Allan deviation of 10^{-11} at one hour.

But the benefits afforded by vibrating RF MEMS technology go far beyond mere component replacement. In fact, the extent to which they offer performance and economic benefits grows exponentially as researchers and designers begin to perceive these devices more as on-chip building blocks than as discrete stand-alone devices. In particular, by mechanically linking vibrating mechanical structures into more general networks, “integrated mi-

cro-mechanical circuits” can be conceived capable of implementing virtually any signal processing function presently realizable via transistor circuits, and with potential power and linearity advantages, especially for functions that involve frequency processing. In essence, micromechanical linkages might form the basis for an integrated micromechanical circuit technology with a breadth of functionality not unlike that of transistor integrated circuits. Among the application possibilities are reconfigurable RF channel-selecting filter banks, ultra-stable reconfigurable oscillators, frequency domain computers, and frequency translators. When further integrated together with other microscale devices (e.g., transistors, micro-ovens, micro-coolers, atomic cells), system-level benefits for portable applications abound, particularly those for which architectural changes allow a designer to trade high Q for lower power consumption and greater robustness, with potentially revolutionary impact.

This overview paper describes not only the MEMS technologies that have achieved some of the abovementioned performance marks, but also what other capabilities their integration density might enable for timing and frequency control in the coming years. It particularly considers mechanical circuit concepts based on this technology, first presenting early mechanical circuit examples, and then attempting to suggest the MEMS technologies and attributes most suitable to enabling a generalized integrated micromechanical circuit platform. The paper ends with a discussion of some of the key practical implementation issues that must be overcome if MEMS technology for timing and frequency control is to be commercialized on a large scale.

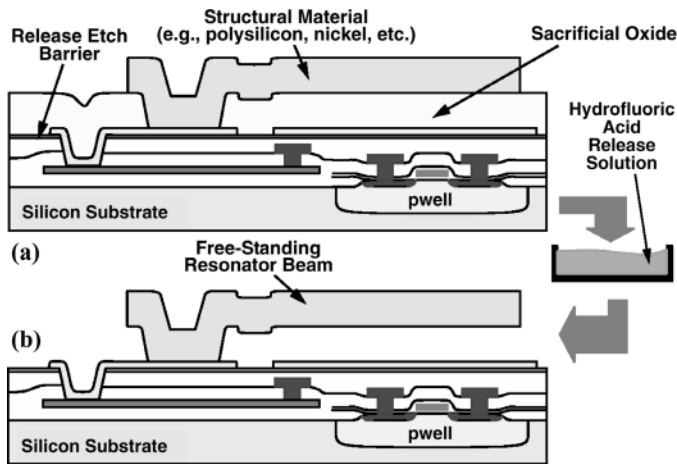


Fig. 2. Cross sections (a) immediately before and (b) after release of a surface-micromachining process done directly over CMOS [14].

II. MEMS TECHNOLOGY

There are now a wide array of MEMS technologies capable of attaining on-chip microscale mechanical structures, each distinguishable by not only the type of starting or structural material used (e.g., silicon, silicon carbide, glass, plastic, etc.), but also by the method of micromachining (e.g., surface, bulk, three-dimensional (3-D) growth, etc.), and by the application space (e.g., optical MEMS, bio MEMS, etc.). For the present focus on timing and portable communications, MEMS technologies amenable to low capacitance merging of micromechanical structures together with integrated transistor circuits are of high interest.

To this end, Fig. 2 presents key cross sections describing a polysilicon surface micromachining process done directly over silicon CMOS circuits in a modular fashion, where process steps for the transistor and MEMS portions are kept separate, in distinct modules. (Modularity is highly desirable in such a process, because a modular process can more readily adapt to changes in a given module, e.g., to a new CMOS channel length.) As shown, this process entails depositing and patterning films above a finished CMOS circuit using the same equipment already found in CMOS foundries until a cross section as in Fig. 2(a) is achieved. Here, the structural polysilicon layer has been temporarily supported by a sacrificial oxide film during its own deposition and patterning. After achieving the cross section of Fig. 2(a), the whole wafer is dipped into an isotropic etchant, in this case hydrofluoric acid, which attacks only the oxide sacrificial layer, removing it and leaving the structural polysilicon layer intact and free to move.

Fig. 3 presents the SEM of a watch timing oscillator that combines a 16-kHz folded-beam micromechanical resonator with a Q of 50,000 together with sustaining CMOS transistor circuits using the very process flow of Fig. 2, but with tungsten as the metal interconnect in order to accommodate 625°C structural polysilicon deposition temperatures [14]. Although the use of tungsten metallization instead of the more conventional copper and aluminum

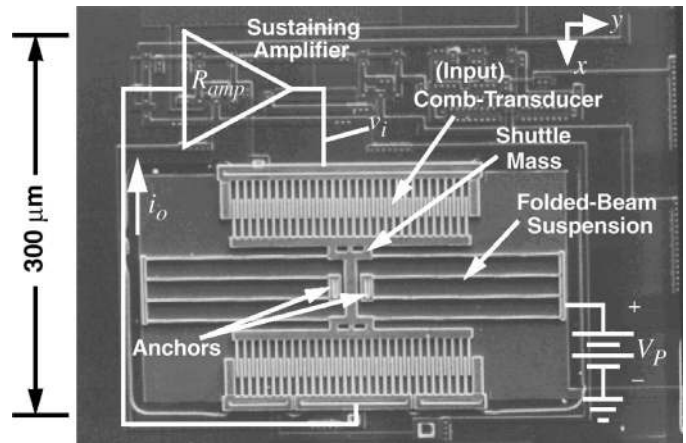


Fig. 3. SEM of a fully integrated 16-kHz watch timekeeper oscillator that combines CMOS and MEMS in a single fully planar process [14].

prevents the process of [14] from widespread use, other variants of this modular process have now been demonstrated that allow more conventional CMOS metals [15]. In addition, other non-modular merging processes [16] have been used in integrated MEMS products for many years now. Whichever process is used, the size and integration benefits are clear, as the complete timekeeper of Fig. 3 measures only $300 \times 300 \mu\text{m}^2$, and could even be smaller if the transistors were placed underneath the micromechanical structure.

III. INTEGRATED MICROMECHANICAL CIRCUITS

The MEMS-enabled integration density illustrated in Fig. 3 has the potential to shift paradigms that presently constrain the number of high- Q components permissible in the design of present-day timing or frequency control functions, and instead allow the use of hundreds, perhaps thousands (or more), of high- Q elements with negligible size or cost penalty. In particular, MEMS technology sports the attributes and ingredients to realize a micromechanical circuit technology that could reach large-scale integrated (LSI), or even very large-scale integrated (VLSI), proportions, the same way integrated circuit (IC) transistors had done over recent decades, and with potential for advances in capabilities in the mechanical domain as enormous as those achieved via the IC revolution in the electrical domain.

Like single transistors, stand-alone vibrating micromechanical elements have limited functionality. To expand their functional range, micromechanical elements (like transistors) need to be combined into more complex circuits that achieve functions better tailored to a specific purpose (e.g., frequency filtering, generation, or translation). Given that the property that allows transistors to be combined into large circuits is essentially their large gain, it follows that mechanical elements can be combined into equally large circuits by harnessing their large Q . As a simple example, transistor elements can be cascaded in

long chains, because their gains compensate for the noise and other losses that would otherwise degrade the signal as it moves down the chain. On the other hand, mechanical elements can be cascaded into long chains because of their extremely low loss—a benefit of their high Q . In essence, if an element has an abundance of some parameter (i.e., gain, Q, \dots), then this can generally be used to build circuits of that element.

Note, however, that the ingredients required for a micromechanical circuit technology comprise much more than just small size. For example, the piezoelectric FBARs [17], [18] that have already become a successful high-volume product in the wireless handset arena, although small, are perhaps not suitable for circuit design, since their frequencies are governed almost entirely by thickness, which is not a parameter that can be specified via computer-aided design (CAD) layout. Given how instrumental CAD has been to the success of VLSI transistor IC design, one would expect CAD amenability to be equally important for micromechanical ICs. In this respect, the resonators and other elements in the repertoire of a micromechanical circuit design environment should have frequencies or other characteristics definable by *lateral* dimensions easily specifiable by CAD.

Continuing on this theme, a more complete set of attributes needed to effect a micromechanical circuit design environment can be listed as follows:

- *CAD-amenable design.* For example, frequencies should be determined by lateral dimensions, which can be specified via CAD, not just vertical dimensions, which cannot. This makes possible an ability to attain many different frequencies in a single layer on a single chip.
- *Geometric flexibility.* Here, a given (often high) frequency should be attainable in a wide variety of shapes (e.g., beams, disks, etc.) and modes.
- *Q 's $> 1,000$ from 1–6000 MHz, with Q 's $> 10,000$ much preferred, if possible.* Q 's this high are needed to allow cascading of circuit blocks without accumulating excessive loss, and to allow channel selection at RF.
- *Thermal and aging stability to better than 2 ppm, or at least amenable to compensation or control to this level.*
- *On/off switchability.* Here, the overriding preference is for vibrating micromechanical devices that can switch themselves, i.e., that do not require extra series switches to do so, and that thus avoid the extra cost and insertion loss.
- *Massive-scale interconnectivity.* In some cases, several levels of both mechanical and electrical interconnect are desired.
- *Nonlinear characteristics* that enable such functions as mixing, amplification, limiting, and other useful signal processing abilities.
- *Amenability to low-capacitance single-chip integration with transistors.* This not only eliminates the issues

with high impedance (to be described), since the tiny magnitudes of on-chip parasitic capacitors allow impedances in the $k\Omega$ range, but also affords designers a much wider palette of mechanical and electrical circuit elements.

A mechanical circuit technology with the attributes mentioned above might make possible filter banks capable of selecting channels (as opposed to just bands) right at RF with zero switching loss; oscillators using multiple high- Q resonators to attain improved long- and short-term stability; oscillators with oven-control-like temperature stability, but consuming only milliwatts of power; ultra-low power completely mechanical RF front ends for wireless handsets; and all of these realized on a single silicon chip.

Before expanding on some of the above, the next section first summarizes the basic resonator building blocks that might be used to implement such mechanical circuits.

IV. VIBRATING MICROMECHANICAL RESONATORS

Among the attributes listed above, the first two, requiring CAD amenability and geometric flexibility, are perhaps the most basic and the most difficult to achieve if constrained to macroscopic machining technologies. In particular, if GHz frequencies were required for flexural mode beams (for which the frequency is governed in part by length—a *lateral* dimension), then a macroscopic machining technology would be hard-pressed to achieve such high frequencies. Fortunately, a major impetus behind MEMS technology stems from the fact that mechanical mechanisms benefit from the same scaling-based advantages that have driven the IC revolution in recent decades. Specifically, small size leads to faster speed, lower power consumption, higher available complexity (leading to increased functionality), and lower cost. And it does so not only in the electrical domain, but in virtually all other domains, including and especially mechanical. Although many examples of this from all physical domains exist, vibrating RF MEMS resonators perhaps provide the most direct example of how small size leads to faster speed in the mechanical domain.

A. High Frequency and Q

For example, on the macro-scale, a guitar string made of nickel and steel, spanning about 25" in length, and tuned to a musical "A" note, will vibrate at a resonance frequency of 110 Hz when plucked. In vibrating at only 110 Hz, and no other frequency, this guitar string is actually mechanically selecting this frequency, and is doing so with a Q on the order of 350, which is ~ 50 times more frequency selective than a typical on-chip electrical LC tank. Of course, selecting a frequency like this is exactly what the RF and IF filters of a wireless phone must do, but they must do so at much higher frequencies, from tens of MHz to well into the GHz range. To achieve such frequencies

with even better mechanical selectivity, dimensional scaling is needed. In particular, by shrinking a guitar string from 25" down to only 10 μm , constructing it in stiffer, IC-compatible materials (such as polysilicon), supporting it at nodes rather than at its ends (to minimize anchor losses), and exciting it electrostatically or piezoelectrically rather than plucking it, one can achieve a free-free beam (FF-beam) resonator such as summarized in row 2 of Table I that resonates at frequencies around 100 MHz with Q 's in excess of 10,000 [20], [23].

In keeping with the scaling-based arguments presented so far, further scaling down to nano-dimensions does indeed yield frequencies in excess of 1 GHz [24]. However, as with nanoelectronics in the electrical domain, there are issues in the mechanical domain that might hinder the use of nanomechanical vibrating resonators (at least in their present form) for today's communication purposes. In particular, excessive scaling may lead to "scaling-induced limitations," such as adsorption-desorption noise [25], temperature fluctuation noise, and insufficient power handling. The first two of these can be mitigated by packaging the device under the right pressure and temperature conditions, but the last of these is perhaps more serious. As with nanoelectronics, the power handling issue with nanomechanical resonators really boils down to an impedance-matching problem. In brief, nanostructures would rather operate at higher impedance levels than their macroscopic counterparts, and in order to interface the nano with the macro (e.g., the antenna), impedance-matching strategies, such as massive arraying of nanostructures, to add their responses might be required. This is not to say that nanomechanical circuits are not practical; they will likely play a larger role if and when needed frequencies begin to approach 50 GHz.

In the meantime, since the majority of today's RF communications occur below 6 GHz, nanoscale flexural mode beams need not be used to interface with macroscopic loads and would instead be better employed as couplers between other elements in a micromechanical circuit. To interface with the macro-world, other geometries that allow GHz frequencies without the need for nanoscale dimensions can be used, such as the 1.51-GHz radial-contour mode disk in row 4 of Table I, which achieves an impressive on-chip room-temperature Q of 11,555 in vacuum, and 10,100 in air. As shown more clearly in the schematic of Fig. 4, this resonator consists of a 20- μm -diameter, 3- μm -thick polydiamond disk suspended by a polysilicon stem self-aligned to be exactly at its center, all enclosed by doped polysilicon electrodes spaced less than 80 nm from the disk perimeter [6]. When vibrating in its radial contour mode, the disk expands and contracts around its perimeter, in a motion reminiscent of breathing [6], [22], and in what effectively amounts to a high-stiffness, high-energy, extensional mode. Since the center of the disk corresponds to a node location for the radial contour vibration mode shape, anchor losses through the supporting stem are greatly suppressed, allowing this design to retain a very high Q even at this UHF frequency.

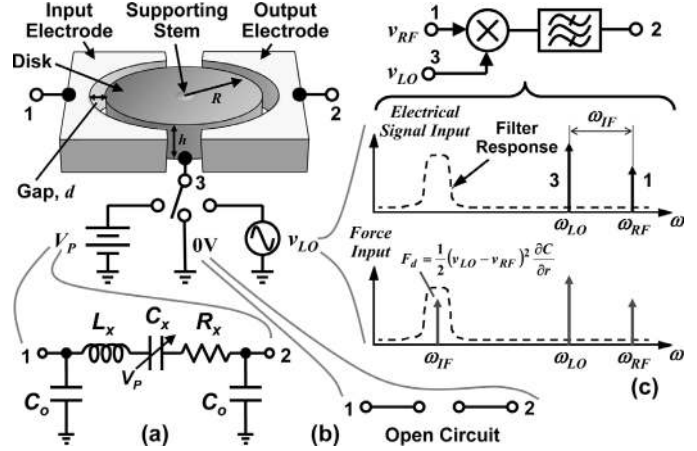
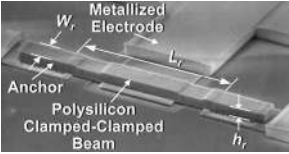
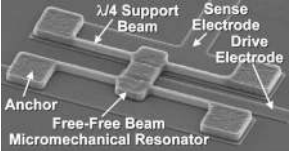
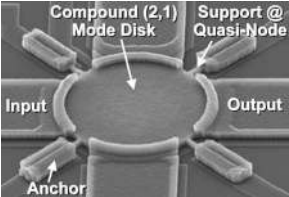
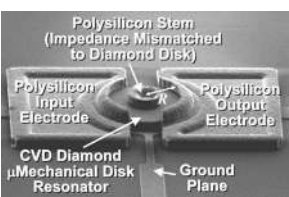
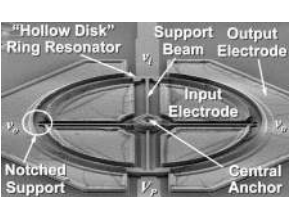


Fig. 4. Perspective-view schematic of the disk resonator of row 4 in Table I, emphasizing the degree to which it is reconfigurable via the voltage applied to its bias port 3. Here, with $V_3 = V_P$, the device is a high- Q LCR; with $V_3 = 0$ V, the device is an open circuit (i.e., is "off"); and with $V_3 =$ a local oscillator signal v_{LO} , the device becomes a mixer [28].

In addition to the GHz data shown in row 4 of Table I, a version of this device at 498 MHz achieves a Q of 55,300 in vacuum [6], which corresponds to a frequency- Q product of 2.75×10^{13} —the highest for any on-chip resonator in the GHz range at room temperature. The astonishingly high Q at greater than GHz frequencies is a result of not only the sheer symmetry of this disk design, but also a strategic impedance mismatch between the polydiamond disk and the polysilicon stem, both of which greatly suppress energy loss through the disk anchor [6]. Furthermore, the high stiffness of its radial contour mode gives this resonator a much larger total (kinetic) energy during vibration than exhibited by previous resonators, making it less susceptible to energy losses arising from viscous gas damping, hence, allowing it to retain Q 's $> 10,000$ even at atmospheric pressure. This resonator not only achieves a frequency applicable to the RF front ends of many commercial wireless devices, but also removes the requirement for vacuum to achieve high Q , which should greatly lower cost. Since the resonance frequency of this device goes approximately as the inverse of its radius, even higher frequency (> 10 GHz) with similar Q 's is expected through radial scaling and the use of higher radial modes.

As detailed in [6], the use of diamond as the structural material for the radial mode resonator of row 4 in Table I contributes to the ease with which it achieves high frequency, since diamond's acoustic velocity is twice that of silicon. However, diamond is not necessary to achieve Q 's greater than 10,000 at frequencies past 1 GHz. Rather, as long as a properly impedance-mismatched resonator-to-anchor transition can be attained, polysilicon also works well, as demonstrated by the "hollow disk" extensional-mode ring resonator, shown in row 5 of Table I [7], [26], [27]. This device uses a centrally located support structure, attached to the ring at notched nodal locations and designed with dimensions corresponding to a quarter-

TABLE I
HIGH FREQUENCY Q PRODUCT VIBRATING RF MEMS DEVICES.

Row	Resonator Type and Description	Photo	Performance
1	<u>Clamped-Clamped Beam</u> [19]: Flexural-mode beam fixed to the substrate at both ends. Micron-scale (i.e., 2- μm -thick) version is simple and works well below 30 MHz. Anchor losses reduce Q as frequency increases beyond 30 MHz. <u>At right:</u> 40- μm -long 7.8-MHz beam.		Demo'ed: $Q \sim 8,000$ @ 10 MHz (vac) $Q \sim 50$ @ 10 MHz (air) $Q \sim 300$ @ 70 MHz (anchor diss.) Q drop w/freq. limits freq. range Series Resistance, $R_x \sim 5\text{--}5,000 \Omega^*$
2	<u>Free-Free Beam</u> [20]: Beam supported at flexural-mode nodal locations by quarter-wavelength torsional supports that “virtually levitate” the device, suppressing losses to anchors. Q remains high in vacuum as frequencies increase past 100 MHz. <u>At right:</u> 14.3- μm -long 82-MHz beam.		Demo: $Q \sim 28,000$ @ 10–200 MHz (vac) $Q \sim 2,000$ @ 90 MHz (air) No drop in Q with freq. Freq. Range: >1 GHz; unlimited w/scaling and use of higher modes Series Resistance, $R_x \sim 5\text{--}5,000 \Omega^*$
3	<u>Wine-Glass Disk</u> [21]: Disk vibrating in the compound (2,1) mode. Can use either a center stem or perimeter supports. With quarter-wavelength perimeter supports located at radial nodal locations, achieves the highest Q 's of any VHF on-chip resonator. <u>At right:</u> 26.5- μm -radius 73-MHz disk with perimeter supports.		Demo'ed: $Q \sim 161,000$ @ 62 MHz (vac) $Q \sim 8,000$ @ 98 MHz (air) Perimeter support design nulls anchor loss to allow extremely high Q Freq. Range: >1 GHz w/scaling Series Resistance, $R_x \sim 5\text{--}5,000 \Omega^*$
4	<u>Contour-Mode Disk</u> [6], [22]: Disk vibrating in the radial-contour mode supported by a stem located at its center nodal point. Use of a material-mismatched stem maximizes the Q , allowing this design to set the record in frequency- Q product for any on-chip UHF resonator at room temperature. <u>At right:</u> 10- μm -diameter 1.5-GHz (in 2 nd mode vibration) CVD diamond disk.		Demo'ed: $Q \sim 11,555$ @ 1.5 GHz (vac) $Q \sim 10,100$ @ 1.5 GHz (air) Balanced design and material mismatching anchor-disk design nulls anchor loss Freq. Range: >1 GHz; unlimited w/scaling and use of higher modes Series Resistance, $R_x \sim 50\text{--}50,000 \Omega^*$
5	<u>Spoke-Supported Ring</u> [7]: Ring supported by spokes emanating from a stem anchor at the device center. Quarter-wavelength dimensioning of spokes nulls losses to the stem anchor, allowing this design to achieve the highest Q 's past 1 GHz of any on-chip resonator. <u>At right:</u> 51.3- μm -inner and 60.9- μm -outer radii ring that attains 433 MHz in its 2 nd contour mode.		Demo'ed: $Q \sim 15,248$ @ 1.46 GHz (vac) $Q \sim 10,165$ @ 1.464 GHz (air) $\lambda/4$ notched support nulls anchor loss Freq. Range: >1 GHz; unlimited w/scaling and use of higher modes Series Resistance, $R_x \sim 50\text{--}5,000 \Omega^*$

*Small values of R_x can be achieved using large dc-bias values and very small gaps, albeit at the cost of linearity.

wavelength of the ring resonance frequency, in order to reflect vibrational energy away from the central anchor and back into the ring. The ring itself vibrates extensionally by expanding and contracting along its inner and outer perimeter edges in a mode shape that allows very high frequency. With this design strategy, this polysilicon ring resonator achieves a Q of 15,248 at 1.46 GHz, which is the highest Q to date past 1 GHz for any on-chip resonator at room temperature [7]. The device is amenable to much higher frequency as well, with a resonance frequency determined primarily by the width of the ring and largely decoupled from its average radius. The fact that frequency does not depend strongly upon average radius allows a designer to specify the ring's perimeter sidewall surface area independently of its frequency. As will be shown in the next section, this equates to being able to specify the ring's impedance by merely choosing an appropriate average radius without affecting its frequency—a useful design feature not shared by the disk resonator of row 4 in Table I.

Fig. 5 presents a graph showing how the frequency- Q product, a common figure of merit for resonators, has in-

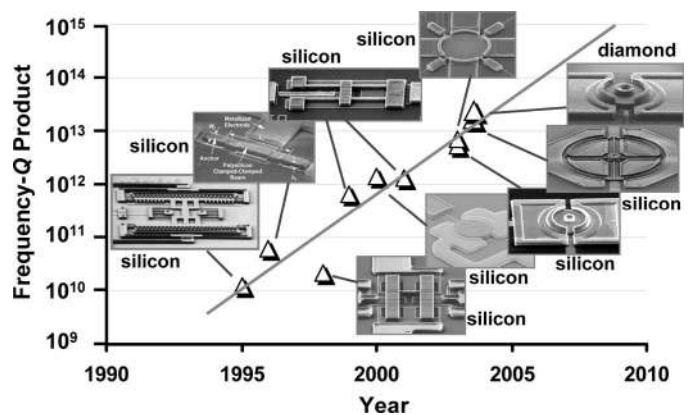


Fig. 5. Plot showing exponential growth in the frequency- Q product of micromechanical resonators over time.

creased exponentially over recent years. As mentioned, micromechanical disk resonators in chemical vapor deposited (CVD) diamond structural material presently hold the record for frequency- Q product, with a value of 2.75×10^{13}

[6]. At the current rate of progress, the prospects for on-chip resonators operating past 10 GHz with Q 's $> 10,000$ are not unreasonable in the next three years.

B. Capacitive Transduction

Note that Table I contains all capacitively transduced devices, which in general offer the best frequency- Q products among micromechanical resonator types, since they generally are constructed in single high quality materials, and thus suffer less from the material interface losses that can encumber other transducer types (e.g., piezoelectric). In addition to better Q , capacitive transduction also offers more flexible geometries with CAD-definable frequencies, voltage-controlled reconfigurability [28], [29], voltage-controlled frequency tunability [30] (that dwindles as frequencies go higher [22]), better thermal stability [8], material compatibility with integrated transistor circuits, and an on/off self-switching capability [29], all of which contribute to the list of mechanical circuit-amenable attributes of the previous section.

The inherent on/off switchability (or “self-switching”) of a capacitively transduced device follows directly from the physics governing the output current sourced by such a device. In particular, to operate the disk of Fig. 4, the mechanical structure must be charged, in this case via the dc-bias voltage V_P (from which no dc current flows once the conductive structure is charged, so there is no dc power consumption). The voltage V_P generated by the charge effectively amplifies both the force imposed by the ac excitation signal v_i (applied to port 1) and the output motional current i_o generated (at port 2) by the dc-biased time-varying electrode-to-resonator capacitor that results when the disk vibrates. The transfer function from input voltage to short-circuited output current can be expressed as

$$\frac{i_o(s)}{v_i(s)} = \frac{1}{R_x} \frac{(\omega_o/Q)s}{s^2 + (\omega_o/Q)s + \omega_o^2}, \quad (1)$$

where ω_o is the resonator's radian resonance frequency, and R_x is its series motional resistance, given by

$$R_x = \frac{\sqrt{m_r k_r}}{Q} \frac{1}{V_P^2} \left[\frac{\varepsilon A_o}{d_o^2} \right]^2 = \frac{\sqrt{m_r k_r}}{Q} \frac{1}{V_P^2} \left[\frac{2\pi \varepsilon h R}{d_o^2} \right]^2, \quad (2)$$

where m_r and k_r are the equivalent mass and stiffness on the perimeter of the disk, respectively; ε is the permittivity in the electrode-to-resonator gap; R and h are the disk radius and thickness, respectively, defined in Fig. 4; d_o is the electrode-to-resonator gap spacing; and A_o is the electrode-to-resonator overlap area. Recognizing (1) as the transfer function for a classic bandpass biquad, when a finite V_P is applied to its resonant structure (i.e., when switched “on”), the two-port micromechanical resonator of Fig. 4 can be modeled by the equivalent LCR electrical circuit shown in part (a) of the figure.

From (2), when the dc-bias V_P is set to 0 V, the series motional resistance R_x goes to infinity, making this device

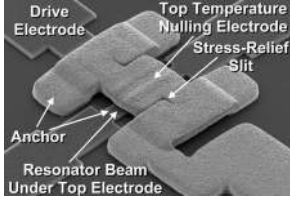
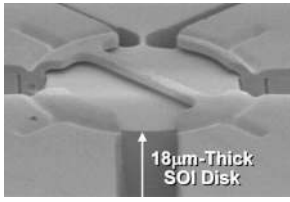
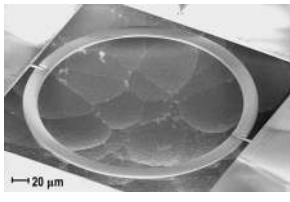
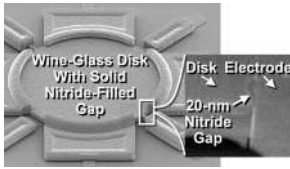
an effective open circuit, as depicted by Fig. 4(b). Thus, while other resonators require a (lossy) switch in series to be switched in or out of an electrical path, a capacitively transduced micromechanical resonator can be switched in or out by mere application or removal of the dc-bias V_P applied to its resonant structure. Note that this can now be done via a simple transistor switch (e.g., a pass gate), since this switching function is out of the signal path, making switch loss a non-issue.

C. Thermal Stability, Aging, and Impedance

Besides frequency range and Q , thermal stability, aging/drift stability, and impedance are also of utmost importance. Table II presents some of the micromechanical resonator devices designed specifically to address these parameters. In particular, the fixed-fixed beam device of row 1 in Table II utilizes a temperature-tailored top electrode-to-resonator gap spacing to attain a total frequency deviation over 27–107°C of only 18 ppm, which actually betters that of AT-cut quartz. This, combined with recent demonstrations of good aging and drift [9], [10], makes micromechanical resonators excellent candidates for reference oscillator applications in communication circuits. In addition, the devices of rows 2 and 3 illustrate strategies for lowering the impedances of stand-alone resonators, the first based on enlargement of the electrode-to-resonator capacitive overlap area to increase electromechanical coupling [31], [32] (i.e., increasing A_o in (2)); and the second dispending with capacitive transducers, and using piezoelectric transducers [33], [34], with the latter being the more successful in achieving the 50–377 Ω impedances desired for matching to off-chip wireless components.

Although it does achieve low impedance, and is amenable to CAD specification, the piezoelectric device of row 3 in Table II still sacrifices the important high Q , on/off self-switching, and temperature stability attributes offered by capacitive transducers. To attain impedances similar to that of the row 3 device, yet retain capacitive transduction and all of its benefits, the device of row 4 has very recently been introduced. This 61-MHz wine-glass mode device is identical in shape and operation to that of row 3 in Table I, but is now equipped with a solid dielectric-filled capacitive transducer gap (to replace the previous air gap) that reduces its impedance by 8 times over its air-gap counterpart, while allowing it to retain a very high Q of 25,300 [35]. In addition to lower motional resistance, the use of solid dielectric-filled transducer gaps is expected to provide numerous other practical advantages over the air gap variety, since it (1) better stabilizes the resonator structure against shock and microphonics; (2) eliminates the possibility of particles getting into an electrode-to-resonator air gap, thereby removing a potential reliability issue; (3) greatly improves fabrication yield by eliminating the difficult sacrificial release step needed for air gap devices; and (4) facilitates larger micromechanical circuits (e.g., bandpass filters comprised of interlinked resonators) by stabilizing constituent resonators as the cir-

TABLE II
THERMAL STABILITY AND IMPEDANCE OF MICRORESONATORS.

Row	Resonator Type and Description	Photo	Performance
1	<p><u>Electrical Stiffness Compensated CC-Beam</u> [8]: CC-beam resonator like that of row 1 in Table I, but now with a top metal electrode. The gap between the top electrode and the resonator grows with increasing temperature, lowering the electrical stiffness to counteract frequency changes due to material temperature dependences. <u>At right:</u> 40-μm-long 10-MHz beam under the metal electrode.</p>		<p>Demo'ed: $Q \sim 4,000$ @ 10 MHz (vac) Temperature-tailored gap to effect an electrical stiffness variation that cancels Young's modulus variation 18 ppm freq. variation over 27–107°C</p>
2	<p><u>SOI Silicon Wine-Glass Disk</u> [31], [32]: Wine-glass mode disk like that of row 3 in Table I, but now constructed in a thick SOI silicon structural layer to effect a large electrode-to-resonator capacitive overlap towards lower series motional resistance. <u>At right:</u> 14.6-μm-diameter 149-MHz disk in 18-μm-thick SOI silicon.</p>		<p>WGDisk: $Q \sim 26,000$ @ 149 MHz (air) SiBAR: $Q \sim 40,000$ @ 137 MHz (vac) $Q \sim 3,700$ @ 983 MHz SOI thickness to effect large capacitive overlap for low Series Resistance, $R_x \sim 43.3 \text{ k}\Omega$ @149 MHz @ 17 V</p>
3	<p><u>Lateral Piezoelectric Ring</u> [33]: Ring-shaped AlN piezoelectric resonator using the d_{31} coefficient to convert vertical drive force into lateral displacement. Realizes a CAD-amenable lateral mode resonator with an efficient piezoelectric drive capable of achieving sub-100-Ω impedances. <u>At right:</u> 10-μm-wide ring, 90-μm-inner radius for 473 MHz.</p>		<p>Demo'ed: $Q \sim 2,900$ @ 473 MHz (air) Contour-mode ring-shaped AlN piezoelectric resonator Driven laterally via the d_{31} coeff., so freqs. determined by lateral dims. Series Resistance, $R_x \sim 80 \Omega$</p>
4	<p><u>Solid-Gap Disk Resonator</u> [35]: Wine-glass mode disk like that of row 3 in Table I, but now using a solid-dielectric filled electrode-to-resonator gap to increase the gap permittivity towards higher actuation force and output current, hence, lower series motional resistance. <u>At right:</u> 32-μm-radius disk with 20-nm nitride-filled gap.</p>		<p>Demo'ed: $Q \sim 25,300$ @ 61 MHz (vac) Solid nitride-filled electrode-to-resonator gap (20 nm) Much better yield and able to achieve low impedance at low dc-bias voltage Series Resistance, $R_x \sim 1.5 \text{ k}\Omega$ @ 4 V</p>

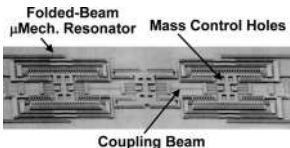
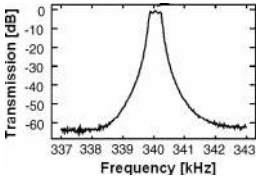
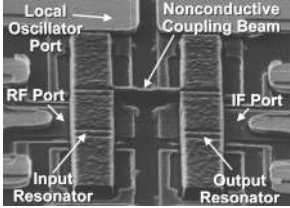
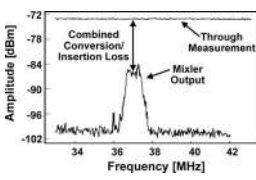
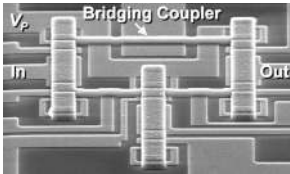
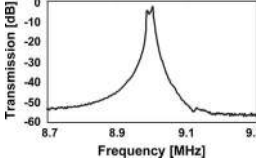
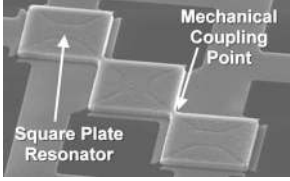
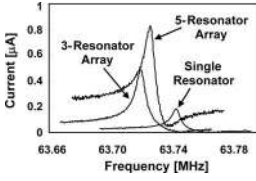
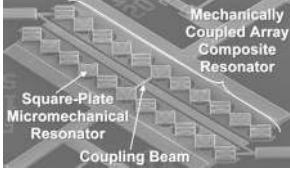
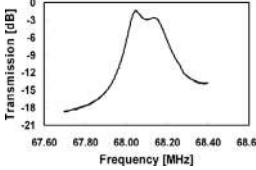
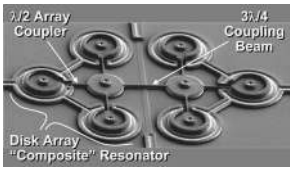
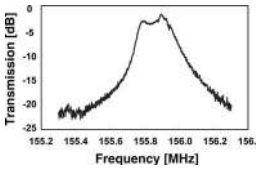
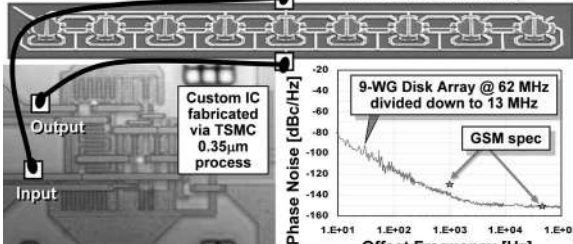
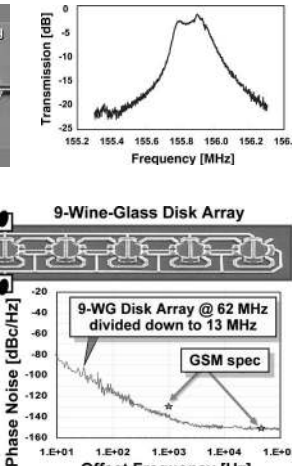
cuits they comprise grow in complexity. Solid-dielectric capacitively transduced resonators employing a vertical-to-lateral drive, and thereby not requiring a nanoscale *lateral* gap, have also been successfully demonstrated [36].

V. MICROMECHANICAL CIRCUIT EXAMPLES

Given that they satisfy all of the attributes listed in Section III, it is no surprise that capacitively transduced resonators have been used to realize the most complex micromechanical circuits to date. Table III summarizes several micromechanical circuits, from bandpass filters with impressive on-chip insertion losses of only 0.6 dB for 0.09% bandwidth, some using non-adjacent bridging to effect loss poles [38]; to mixer-filter (“mixler”) devices that both translate and filter frequencies via a single passive structure [28]; to impedance transforming mechanically coupled arrays that combine the responses of multiple high-impedance resonators to allow matching to a much lower 50 Ω [39]; to filters using mechanically coupled composite resonators to allow matching to 50 Ω while attaining the lowest insertion loss to date for VHF micromechanical filters [40], [41].

Each of the filters in Table III is comprised of several identical resonator elements coupled by mechanical links attached at very specific locations on the resonators. As detailed more fully in [19] and [37], the center frequency of such a mechanical filter is determined primarily by the (identical) frequencies of its constituent resonators, while the spacing between modes (i.e., the bandwidth) is determined largely by a ratio of the stiffnesses of its coupling beams to that of the resonators they couple at their attachment locations. The circuit nature of each filter in Table III is emphasized by the fact that each was designed using equivalent electrical circuits defined by electromechanical analogies [19], [37], which allowed the use of electrical circuit simulators, like SPICE (Dept. of Electrical Engineering and Computer Sciences, University of California at Berkeley, Berkeley, CA)—an important point that implies mechanical circuits should be amenable to the vast automated circuit design environments already in existence. Fig. 6 presents the specific electric circuit equivalence for the bridged filter of row 3 of Table III, where each flexural-mode resonator equates to an *LCR* circuit; each coupling beam is actually an acoustic transmission line, so equates to a *T*-network of energy storage elements, just like an

TABLE III
SUMMARY OF VIBRATING MICROMECHANICAL CIRCUITS.

Row	Mechanical circuit description	Photo	Data	Performance
1	<u>3-Resonator Folded-Beam Filter</u> [37]: 3 identical folded-beam comb-driven resonators coupled by flexural-mode beams attached to low velocity locations. Established many of the basic design strategies for micromechanical filters. <u>At right:</u> total length of $\sim 300 \mu\text{m}$.			Freq. = 340 kHz BW = 403 Hz %BW = 0.09% StopB Rej. = 64 dB Ins. Loss < 0.6 dB
2	<u>Mixer-Filter</u> [28]: Filter structure using CC-beam resonators coupled by a flexural mode beam that uses the square-law voltage-to-force transfer function of a capacitive transducer to mix input signals down to a mechanical force. <u>At right:</u> 18.8- μm -long CC-beams for 37 MHz.			Mixes a 240-MHz RF down to 37-MHz IF, then filters Conv. Loss = 9.5 dB %BW = 1.7% Ins. Loss = 3.5 dB
3	<u>3-Resonator Bridged CC Beam</u> [38]: Couples non-adjacent resonators (in addition to adjacent ones) to introduce a loss pole into the filter characteristic toward an improved shape factor. <u>At right:</u> 40- μm -long CC-beams for 9 MHz.			Freq. = 9 MHz BW = 20 kHz %BW = 0.2% StopB Rej. = 51 dB Ins. Loss < 2.8 dB
4	<u>Mechanically-Coupled Resonator Array</u> [39]: An array of transverse-mode square resonators strong-coupled mechanically at their corners so that all resonators vibrate at a single mode frequency, with other modes suppressed by electrode phasing. <u>At right:</u> 16- μm sides for 64-MHz square.			Automatic matching of resonators achieved via mech. coupling; current multiplied by number of resonators N
5	<u>Array Composite Filter</u> [40]: Two 11-square array composite resonators coupled by a flexural-mode spring to realize a 2-resonator filter with an array-reduced input impedance matchable to 50 Ω . <u>At right:</u> 16- μm sides for 68-MHz constituent square resonators.			Freq. = 68.1 MHz BW = 190 kHz %BW = 0.28% StopB Rej. = 25 dB Ins. Loss < 2.7 dB
6	<u>Disk Array Composite Filter</u> [41]: Two 4-disk array composite resonators coupled by an extensional-mode beam to realize a 2-resonator filter with an array-reduced input impedance. Triangular placement of disks suppresses spurious modes. <u>At right:</u> 17- μm -radius disks for 156 MHz.			Freq. = 156 MHz BW = 201 kHz %BW = 0.13% StopB Rej. = 22 dB Ins. Loss < 2 dB
7	<u>Disk Array Composite Oscillator</u> [11]: 9-wine-glass disk array resonator embedded in a positive feedback loop with a custom-designed IC sustaining amplifier. The use of an array composite tank element raises power handling while retaining $Q > 100,000$ allowing this oscillator to meet GSM phase noise specifications. <u>At right:</u> 32- μm -radius disks for 62 MHz.			Freq. = 62 MHz 9-Wine-Glass-Disk Composite Array Resonator $w/Q = 118,900$ Custom IC $L\{f_m = 1 \text{ kHz } f/13 \text{ MHz}\} = -138 \text{ dBc}$ $L\{f_m = 10 \text{ kHz } f/13 \text{ MHz}\} = -151 \text{ dBc}$

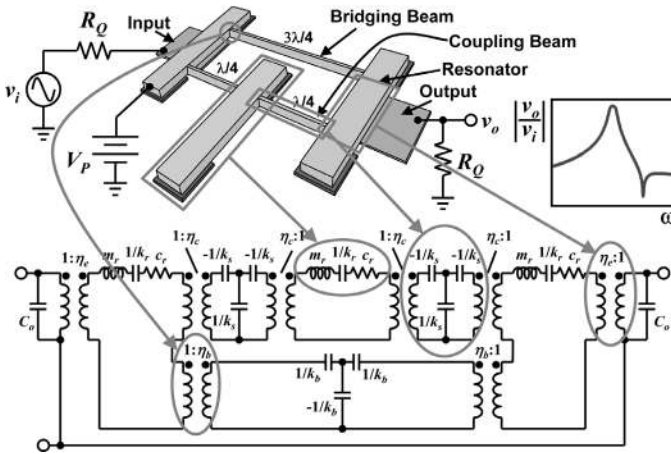


Fig. 6. Equivalent circuit and explicit mechanical-to-electrical equivalence for the bridged micromechanical filter of row 3 in Table III.

electrical transmission line; the attachment locations of couplers to resonators must be chosen carefully, since they actually realize velocity transformations, which can again be modeled by transformers; the capacitive electromechanical transducers at the input and output ports equate to electrical transformers; and all circuit elements are specified by the lateral dimensions of their associated mechanical elements, making the whole structure amenable to automatic generation by a CAD program. Such a program could also automatically generate the layout required to achieve a specific filter specification, making the realization of a VLSI circuit of such filters as simple as already done for VLSI transistor ICs.

Although the filter of row 3 exhibits excellent in-band insertion loss and stopband rejection, it requires a matching input termination impedance larger than 50Ω , making it unsuitable for placement directly after an antenna. As mentioned in Section IV, this is a consequence of the use of weak air-gap capacitive transducers, which can be remedied by using some of the methods presented in Table II [33], [35], [36]. But there is another, perhaps more elegant, circuit-based remedy based on arraying. In particular, the arraying used in the devices of rows 4 and 5 not only provides a lower filter termination impedance by increasing the effective capacitive transducer overlap area, but also raises the 3rd-order intermodulation intercept point (IP_3) of the composite device [39], [42]–[44] (i.e., raises its linearity) in the process. Note that the device in row 4 of Table III is not just an array of stand-alone square resonators; rather, the resonators are actually mechanically coupled to form a “composite” resonator in which all constituent resonators vibrate at exactly the same electrode-specified mode frequency, allowing their outputs to be combined in phase. With an output equal to the sum of its resonator outputs, an N -resonator array composite exhibits an N times lower motional resistance and a substantially larger power handling capability than a stand-alone resonator, while still maintaining a comparable Q . In essence, arraying reduces motional resistance by raising the overlap area term A_o in (2). Fig. 7 illustrates how arraying can achieve a

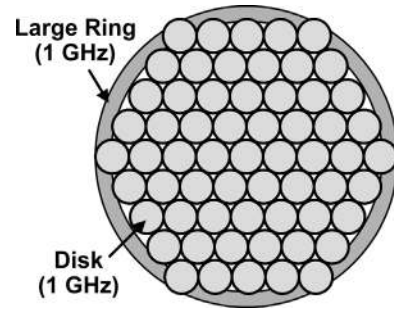


Fig. 7. Illustration showing that, in the same footprint, an array of small 1-GHz disks can achieve a larger sidewall surface area (hence, larger electromechanical coupling and smaller filter impedance) than a single 1-GHz ring made large to minimize impedance.

much larger increase in capacitive transducer overlap area than a single device specially designed for larger transducer area—a clear example of how a circuit technique can be superior to the use of a single “advanced” device.

The similarities between the described arraying approach and similar strategies in transistor integrated circuit design are noteworthy. In particular, the use of an array of resonators to match the impedance of a micromechanical circuit to an off-chip macroscopic element (e.g., an antenna) is really no different from the use of a cascade of progressively larger inverters (or in actual layout, arrays of smaller inverters) to allow a minimum-sized digital gate to drive an off-chip board capacitor. In essence, micro- (or nano-) scale circuits, whether they be electrical or mechanical, prefer to operate with higher impedances than macro-scale ones, and interfacing one with the other requires a proper impedance transformation. In a building block circuit environment, such an impedance transformation is most conveniently accomplished via large numbers of circuit elements, whether they be electronic transistors or mechanical resonators.

Again, it is the amenability to CAD of vibrating RF MEMS technology that makes the purely mechanical filters and arrays of Table III possible, and it is this same amenability to CAD that stands to effect substantial reductions in both cost and size for multiband, multimode transceivers like that of Fig. 1. In particular, the tiny size and high integration density of micromechanical circuit technology makes the chip of Fig. 8 possible, which includes all of the high- Q filters and resonators of Fig. 1 in a chip size of only $0.25 \text{ mm} \times 0.5 \text{ mm}$. Furthermore, if the on-chip passives technology used in Fig. 8 is indeed one where device properties (e.g., frequencies) can be specified by CAD-definable quantities (e.g., lateral dimensions, as opposed to thickness), allowing them to be defined in a single deposited layer, then the cost of a single chip of all 11 of the high- Q passives in Fig. 1 could potentially end up being about the same as *one* of the original off-chip passives. Needless to say, this degree of cost reduction creates great incentive for development of lateral vibration-mode MEMS resonators, for which frequency is defined by CAD-definable lateral dimensions; as opposed to thickness

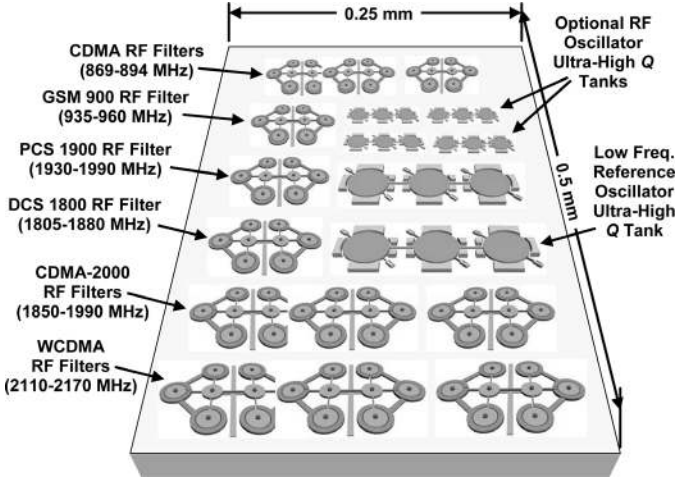


Fig. 8. Schematic of a single chip of high- Q passives made possible by lateral-mode vibrating MEMS resonator technology. Here, a resonator technology that allows many different frequencies to be defined (e.g., via CAD layout) in a single film layer is assumed. The 0.25×0.5 -mm² chip includes the receive path high- Q passives of Fig. 1, plus additional oscillator tanks for improved phase noise and injection locking suppression. Although only receive path high- Q filters are included here, note that transmit filters, as well as other lateral-dimension-defined passives described in this paper, could also be added while still retaining a tiny chip size.

mode resonators (e.g., FBARs or shear-mode quartz) that require a different film thickness for each individual frequency, and thus impose higher cost. If the lateral-mode resonators further use capacitive transduction, then they possess the additional advantage of self-switchability [9], which allows the system of Fig. 1 to dispense with the multi-throw switch and, hence, dispense with its size, cost, and insertion loss.

In addition to presenting various mechanical circuits, Table III implicitly indicates the progression of micromechanical circuit complexity with time. In particular, the composite array filter in row 5 uses more than 43 resonators and links, which approaches a medium-scale integrated (MSI) micromechanical circuit. The hierarchical design methodology used for this circuit, which consists of two 11-resonator array composites coupled by a flexural mode coupling spring, should be applicable to even larger integration densities, perhaps inevitably leading to LSI or VLSI mechanical circuits, such as will be described in Section VIII. When combined with transistor integrated circuits (preferably on the same chip [14]–[16]), the time domain prowess of transistors can be merged with the frequency domain capabilities of mechanical circuits to achieve even greater functionality.

VI. MICROMECHANICAL RESONATOR OSCILLATORS

Leeson's equation [45] indicates that the stability of an oscillator, as measured by its phase noise, is inversely proportional to the Q of its frequency-setting tank element. Given that the micromechanical disk and ring resonators

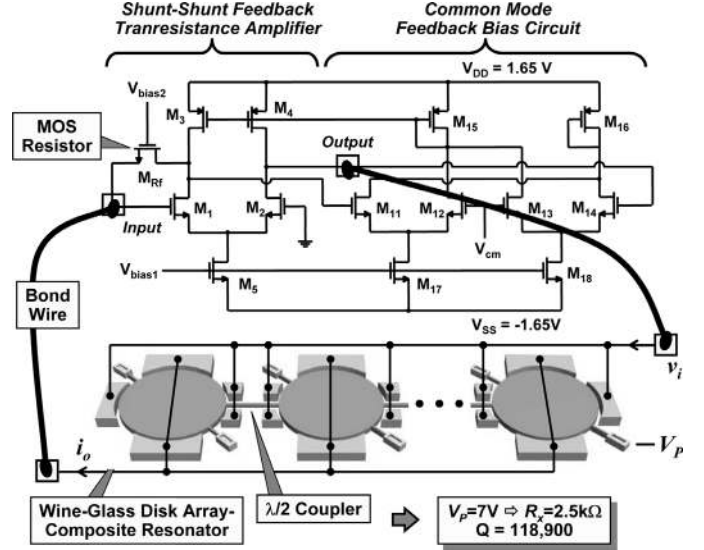


Fig. 9. Circuit schematic of the 62-MHz series resonant reference oscillator of row 7 of Table III using a 9-wine-glass disk array composite resonator frequency-setting element with a Q of 118,000 in vacuum [11].

of rows 4 and 5 of Table I have posted the highest room temperature Q 's of any on-chip resonator around 1 GHz to date, the use of MEMS technology in compact local oscillator (LO) implementations is fully expected to yield substantial improvements in LO performance. In particular, according to Leeson's equation, if a present-day voltage-controlled oscillator (VCO) attains -121 dBc/Hz at a 600-kHz offset from an 1.8-GHz carrier using an LC tank with a Q of 30, then the use of a vibrating micromechanical disk resonator with a Q of 10,000 should provide ~ 50 dB of improvement, or -171 dBc/Hz at a 600-kHz carrier offset (provided the thermal noise floor allows it, that is).

To date, work toward demonstrating the above GHz oscillator using a micromechanical resonator tank is ongoing. In the meantime, the lower frequency reference oscillator in row 7 of Table III [11], based on a 62-MHz wine-glass-mode disk array composite resonator, has recently been demonstrated with an impressive normalized phase noise-fractional offset-power product of -223.4 dB, which is substantially better than the -185.5 dB attained by an LC -based oscillator [46], and still better than the -211.1 dB achieved by a quartz crystal oscillator [47]. As shown in the SEM of row 7 of Table III and by its circuit schematic in Fig. 9, this particular oscillator utilizes a 9-wine-glass-disk array composite resonator, much like that of row 4 of Table III described in the previous section, to achieve a tank element that handles significantly higher power than a stand-alone wine-glass disk, while still retaining a very high Q of 118,900. Again, Leeson's equation [45] indicates that the stability of an oscillator, as measured by its phase noise, is inversely proportional to the Q of its frequency-setting tank element and to the power circulating through the oscillator feedback loop. Thus, the use of a disk array-composite to increase the power- Q product over that of a stand-alone resonator constitutes a mechan-

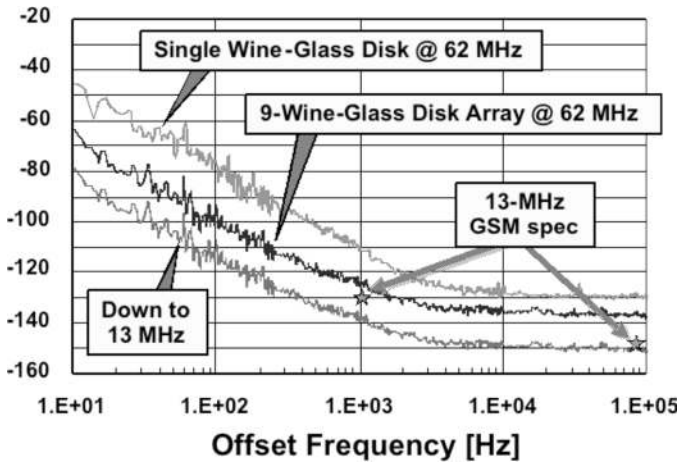


Fig. 10. Comparison of measured phase noise density versus carrier offset for the 62-MHz array composite disk oscillator circuit of row 7 in Table III against that of a 61-MHz stand-alone wine-glass disk oscillator, with an extrapolation for the former down to 13 MHz for evaluation against GSM specs.

ical circuit technique that can very effectively improve the phase noise performance of any oscillator. This mechanical circuit technique has provided up to 40 dB of phase noise improvement for a previous oscillator [48], and is in fact responsible for allowing the oscillator in row 7 of Table III to consume only 350 μW of power toward phase noise marks (shown in Fig. 10) at 1 kHz and far-from-carrier offsets of -123 and -136 dBc/Hz, respectively [11], which are significantly lower than the -110 and -132 dBc/Hz achieved by a version of this oscillator using only a single resonator [12], rather than an array. When divided down to 13 MHz for evaluation against standard specifications, the values for the array composite resonator oscillator equate to -138 and -151 dBc/Hz at 1 kHz and far-from-carrier offsets, respectively, both of which together satisfy the GSM reference oscillator requirement [11]. This result illustrates yet again how the use of many high- Q elements in an interlinked mechanical circuit can propel performance.

Although GSM performance is already very good, there is still room for improvement. In particular, if the $1/f^3$ frequency dependence seen at frequencies below the noise corner in Fig. 10 can be removed, then a significant reduction in phase noise at close-to-carrier frequencies should ensue. As with most other oscillators, the $1/f^3$ noise dependence derives in part from aliasing of $1/f$ noise from the transistor circuit back into the passband of the oscillator. Unlike with crystal oscillators, however, this noise aliasing often arises more through nonlinearity in the micromechanical resonator than in the transistor sustaining circuit. Analytical theory in fact predicts that nonlinearity in the resonator's capacitive transducer generally contributes the largest aliased contribution, as described in [49] and [50]. Interestingly, the theory of [49] and [50] actually do not always completely describe all of the $1/f^3$ noise behavior, in that oftentimes more $1/f^3$ noise is present than can be theoretically generated by aliased transistor $1/f$ noise alone, especially at large resonator displacement amplitudes. It

is possible that $1/f$ noise in the mechanical tank circuit itself could be responsible for the additional noise. On the other hand, since limiting for the oscillator of row 7 in Table III actually occurs via mechanical resonator nonlinearity rather than via the more common transistor nonlinearity, certain aspects of the mechanical limiting mechanism might also contribute to increased noise. Needless to say, a better understanding of noise generation mechanisms in micromechanical resonator oscillators could lead to significantly better oscillator performance, so research in this area is expected to be abundant over the next few years.

In the meantime, recent work along these lines indicates that the $1/f^3$ component can be removed (leaving behind $1/f^2$ noise) by introducing automatic-level-control (ALC) into the sustaining circuit [12], [49]. This allows the oscillator to limit via ALC feedback, not resonator nonlinearity, thereby removing possible noise contributions caused by resonator-based limiting. It also reduces the vibration amplitude of the resonator and, hence, reduces noise aliasing through nonlinearity in its capacitive transducer, which then reduces $1/f^3$ noise [12], [49]. In fact, given that $1/f^3$ noise seems to decrease with the vibration amplitude of the mechanical element, and given that arraying reduces the vibration amplitude needed for the element to source a specified output current magnitude, it is no surprise that the use of a larger number of mechanically coupled resonators in the composite array tank element of the oscillator in Fig. 9 reduces $1/f^3$ noise [11]. That this is the case can be seen by simply comparing the phase noise curves for the 62-MHz single wine-glass disk oscillator and the 62-MHz 9-wine-glass disk array oscillator near the noise corner in Fig. 10. Doing so, one observes that in a small frequency span right below the noise corner, the slope of the 9-wine-glass disk array oscillator's phase noise is clearly $1/f^2$, whereas that of the single wine-glass disk oscillator is $1/f^3$. Since both oscillators used identical sustaining transistor circuits, this result at the very least confirms that the micromechanical tank element plays a significant role in governing oscillator $1/f^3$ phase noise performance. Again, there is much room for further exploration here.

A. Micro-Oven Control

In addition to good short-term stability, MEMS technology has great potential to achieve oscillators with excellent thermal stability. In particular, the tiny size and weight of vibrating micromechanical resonators allow them to be mounted on micro-platforms suspended by long thin tethers with thermal resistances many orders of magnitude larger than achievable on the macro-scale. Such a large thermal resistance to its surroundings then allows the platform and its mounted contents to be heated to elevated temperatures with very little power consumption (e.g., milliwatts). Fig. 11 presents the first such platform-mounted folded-beam micromechanical resonator, where the nitride platform supporting the resonator also included thermistor and heating resistors that, when embedded in a feedback loop, maintained the temperature of the platform

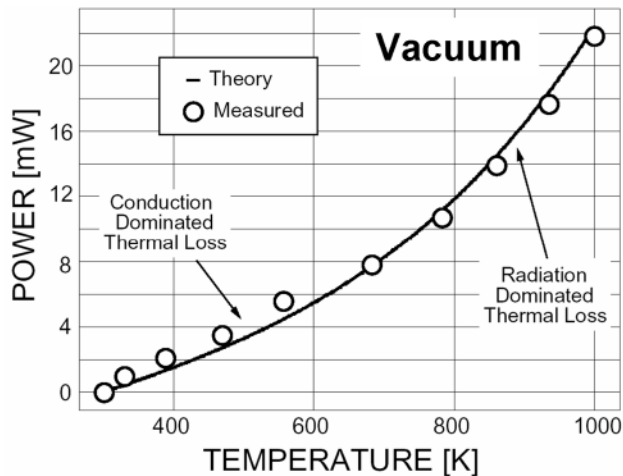
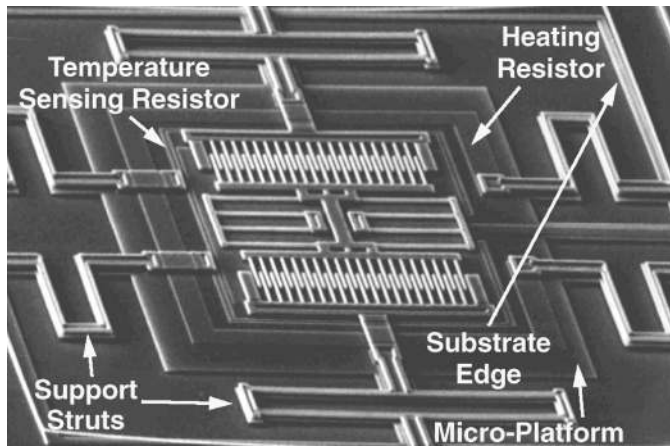


Fig. 11. (top) SEM of a fabricated folded-beam micromechanical resonator mounted on a micro-oven platform. (bottom) Measured power required to achieve a given temperature. Here, only 2 mW are required to achieve 130°C [51].

at 130°C with only 2 mW of total power consumption [51]. With oven-controlling feedback engaged, the temperature coefficient of the platform-mounted micromechanical resonator was reduced by more than 5 times, with thermally induced warping of the platform the performance limiter. Much better reduction factors are expected with a more refined platform design.

VII. TOWARDS CHIP-SCALE ATOMIC CLOCKS

Although the described micromechanical resonator oscillators are expected to achieve excellent phase noise performance at carrier offsets greater than 100 Hz, and micro-oven control might soon allow them to reach temperature stabilities down to 10^{-9} (and maybe even better), their aging rates will likely not match those of atomic clocks. But unless atomic clocks with stability better than 10^{-11} over one hour can be shrunk from the 9,000-cm³, 60-W commercial units existing today, down to a more portable size and battery drain, our best electronic systems (which rely on the accuracy and precision of atomic clocks) will remain on tabletops, and out of the hands of the mo-

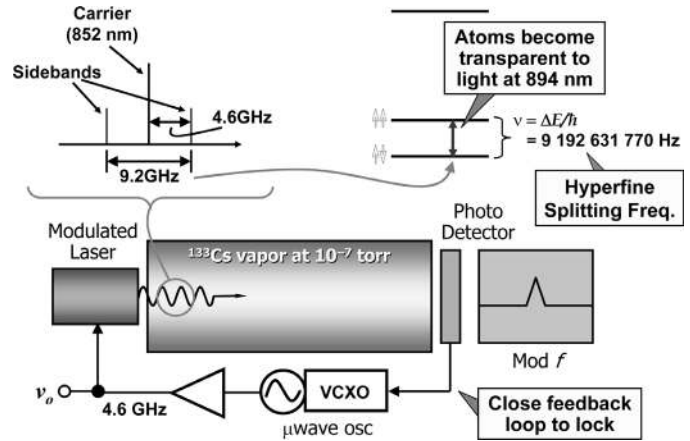


Fig. 12. Schematic describing the basic topology of a vapor cell-based atomic clock, this one exciting the hyperfine resonance via a laser-modulated approach dubbed coherent population trapping (CPT).

bile user. With the intent of changing this, the Chip-Scale Atomic Clock (CSAC) program in the Microsystems Technology Office (MTO) of the Defense Advanced Research Projects Agency (DARPA) in the U.S. is attempting to harness MEMS and microphotonics technologies to miniaturize atomic clocks down to a more-than-portable 1-cc size, while still achieving 10^{-11} Allan deviation over one hour with less than 30 mW of power. These goals represent a more than 9,000 times reduction in volume, and 2,000 times reduction in power consumption, versus the small atomic clocks in the market at the 2002 start of the CSAC program.

Like quartz or vibrating resonator oscillators and clocks, atomic clocks function by generating a very stable frequency off of a very stable reference. The main difference is that a quartz oscillator derives its frequency from a mechanically vibrating reference, which makes its frequency subject to long-term changes in mechanical dimensions and stress. An atomic clock, on the other hand, derives its frequency from the energy difference between the hyperfine states of an alkali metal atom, which is a constant of nature and, thereby, much more predictable and stable.

Among the existing approaches to realizing an atomic clock, the vapor cell method depicted schematically in Fig. 12 is perhaps the most amenable to miniaturization. Here, a cell containing the alkali metal in a sufficiently dense vapor state is interrogated by a laser at a wavelength absorbed by the vapor (i.e., that excites the single outer orbital electron to the next orbital; 894 nm for the cesium D1 line). A photodetector at the other end of the vapor cell monitors the intensity of the laser light. Energy at the frequency that excites the hyperfine transition, given by $\Delta E = h\nu$, where h and ν are Planck's constant and the characteristic frequency, respectively, is then pumped into the system in one of two ways (either of which can work at the microscale): (1) electromagnetically, via an RF signal at frequency ν ; or (2) optically, by modulating the laser at the needed frequency ν . Fig. 12 uses the latter method, where modulation of the laser at the hyperfine

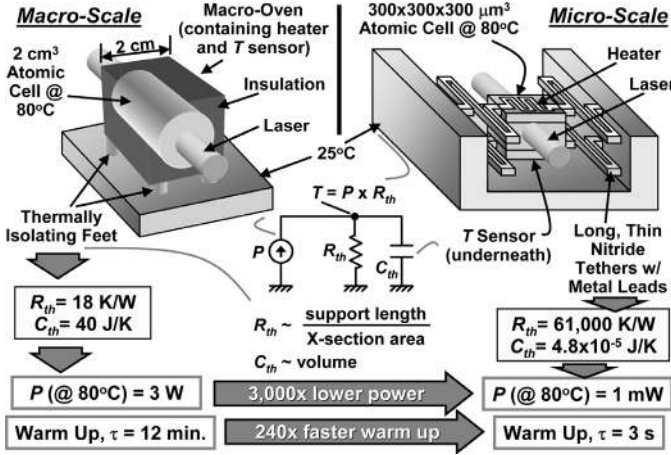


Fig. 13. Schematics summarizing the analytical determination of the powers required to maintain macro and micro vapor cells at 80°C in vacuum. Here, the equivalent thermal circuit used also yields warm up times.

splitting frequency ($\nu = 9.192631770$ GHz, for cesium) excites the atoms into a coherent state, where they become transparent to the interrogating laser light (i.e., they no longer absorb it), inducing a peak in the intensity of the laser light. A microwave oscillator capable of delivering the needed output power is then locked to the (very accurate) hyperfine splitting frequency via a feedback circuit that controls the oscillator frequency so that the photodetector intensity is maximized at the hyperfine peak.

A. Reducing Power Consumption Via Scaling

As mentioned, the alkali metal atoms must be maintained at a sufficient density in a vapor state to operate the atomic clock, which means power must be consumed to heat the vapor cell that contains the atoms. For a tabletop atomic clock, this can take tens of watts of power. Obviously, any approach to reducing the total clock power consumption down to 30 mW must include a strategy for reducing this heating power by three orders of magnitude.

Once again, as with the vibrating resonators of Section IV, smaller is better. In particular, for the case of a vapor cell-based atomic clock, scaling a Cs- or Rb-filled atomic cell to millimeter or even micron dimensions greatly reduces the power required to maintain the cell at the elevated temperature needed to keep the atoms in a sufficiently dense vapor state. The power savings can be enormous, as illustrated in Fig. 13, which compares the powers required to maintain (in vacuum) a temperature of 80°C on a small macro-cell, about 2 cm in diameter, and on a tiny micro-cell, measuring just 300 μm on a side, assuming that conduction is the dominant heat loss mechanism. Given that the microscale cell weighs so little, it can be supported by tethers so long and thin that they can achieve thermal resistances R_{th} on the order of 61,000 K/W, to be compared with the 18 K/W that might be seen on the macroscale. These differences in thermal isolation lead to a micro-cell power requirement for 80°C of only 1 mW,

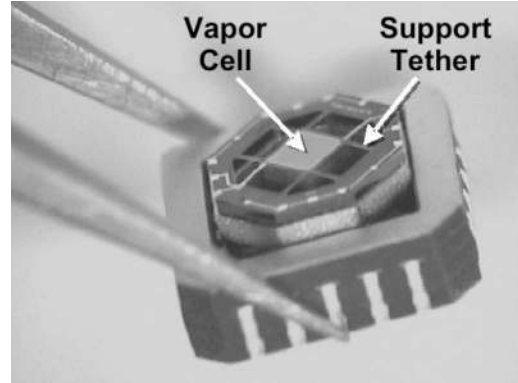


Fig. 14. Tiny physics package by Symmetricom/Draper/Sandia, featuring a tiny atomic vapor cell supported by long thin thermally isolating tethers that allow heating to 80°C with less than 5 mW of heating power.

which is 3000 times smaller than the 3 W that would be required for the small macro-cell. Furthermore, due to the tiny volume of the micro-cell, and thus tiny thermal capacitance on the order of only 10⁻⁵ J/K, the warm up time for the micro-cell of only 3 seconds is 240 times faster than the 12 minutes typical of macro-scale atomic clocks.

It should be noted that the above illustration considered only conductive heat loss for simplicity. In actuality, the conductive heat loss for the tether-supported micro-cell is so small that radiation heat loss becomes dominant at 80°C. This radiation heat loss, however, is also small, so that the actual micro-atomic tether-supported cell by the Symmetricom/Draper/Sandia team in the CSAC program, shown in Fig. 14, still requires only 5 mW of power to maintain a temperature of 80°C in its vacuum enclosure [52].

B. Scaling Limits

But along with its benefits, scaling also introduces some potential disadvantages. In particular, among the more troublesome disruptors of stability in a gas-cell atomic clock are collisions between the atomic gas species and the walls, which can dephase the atoms, disrupting their coherent state. Because shrinking an atomic cell amounts to raising its surface-to-volume ratio, hence, making its walls look much larger to the atoms, one might expect an increase in atom-to-wall collisions to degrade the Q of an atomic cell as it is scaled to millimeter or microscale dimensions. Fortunately, however, the judicious use of the right buffer gases to lower the mean free path of “clock” atoms so that they rarely reach the walls, but rather “soft impact” the buffer gases, allows a designer to shrink vapor cell dimensions down to 100’s of microns while maintaining a low enough atom-to-wall collision rate to allow clock performance down to 10⁻¹¹ Allan deviation at one hour.

Fig. 15 presents photos of one of the smallest physics packages ever built (by NIST [53]), occupying just 10 mm³ in volume, and comprising a tiny micromachined atomic vapor cell [53] containing either Cs or Rb, an interrogat-

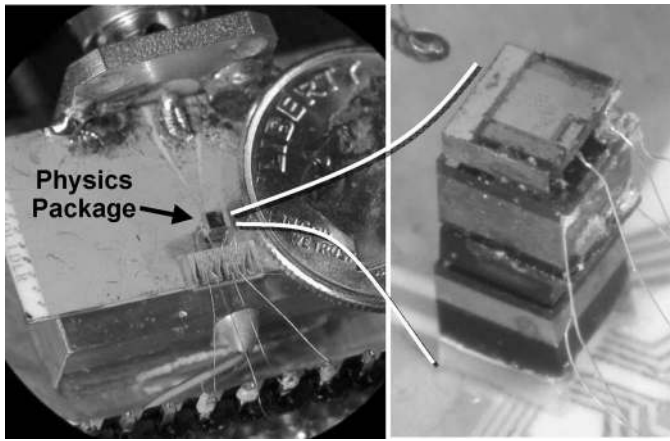


Fig. 15. Chip-scale atomic physics package by NIST, occupying less than 10 mm^3 in volume.

ing vertical-cavity surface-emitting laser (VCSEL) working preferably on the D1 line, a photodiode detector, polarizing and focusing optics, heater elements to maintain atoms in a sufficiently dense vapor state, and a micromechanical suspension system that thermally isolates the vapor cell/heater structure to allow elevated temperatures with low power consumption. The thermal isolation for this physics package is not quite as good as that of Fig. 14, so its power consumption is on the order of 75 mW , but its tiny vapor cell so far has permitted measured Allan deviations better than 10^{-11} at one hour.

C. Tiny Atomic Clocks

Fig. 16 presents the Allan deviation plot and photo of a completely self-contained atomic clock by the Symmetri-com/Draper/Sandia team in the CSAC program that occupies only 9.95 cm^3 , yet achieves an Allan deviation of 5×10^{-11} at 100 s , while consuming less than 153 mW of power. This is the smallest, lowest power atomic clock in existence to date. But it won't remain so long; in particular, if things go as planned in the CSAC program, 1-cm^3 versions consuming only 30 mW while attaining 10^{-11} at one hour Allan deviation will likely surface soon.

VIII. TOWARD LARGE-SCALE INTEGRATED MICROMECHANICAL CIRCUITS

Again, to fully harness the advantages of micromechanical circuits, one must first recognize that due to their microscale size and zero dc power consumption, micromechanical circuits offer the same system complexity advantages over off-chip discrete passives that planar IC circuits offer over discrete transistor circuits. Thus, to maximize performance gains, micromechanical circuits should be utilized on a massive scale. Again, as with transistor circuits, LSI (and perhaps eventually VLSI) mechanical circuits are best achieved by hierarchical design based on building block repetition, where resonator, filter, or mixer-filter

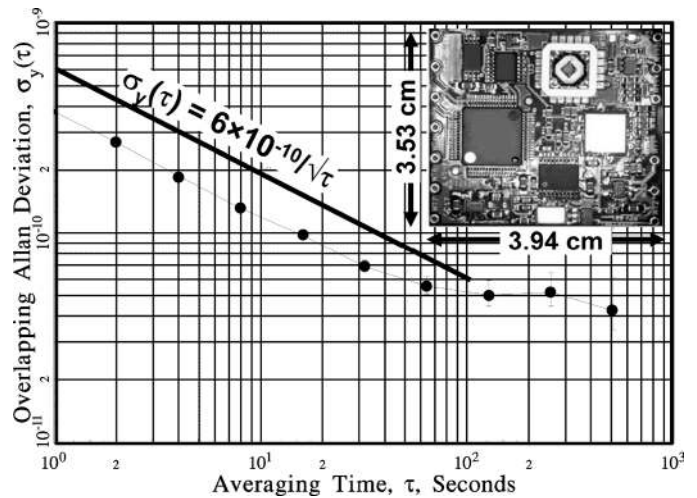


Fig. 16. Measured Allan deviation plot for the output of the 9.95-cm^3 atomic clock by the Symmetri-com/Draper/Sandia CSAC team. (The points are the measured data.)

building blocks might be combined in a fashion similar to that of the memory cell or gate building blocks often used in VLSI transistor ICs.

One example of an LSI micromechanical circuit expected to impact future transceivers is the RF channel selector mentioned in Section I and described at the system level in [4] and [5]. Such an RF channel selector, if achievable, is widely coveted by RF designers. Indeed, if channel selection (rather than band selection) were possible at RF frequencies (rather than just at IF or baseband), then succeeding electronic blocks in the receive path (e.g., low noise amplifier (LNA), mixer) would no longer need to handle the power of alternate channel interferers. This would greatly enhance the robustness of the receiver by raising its immunity against jamming. In addition, without alternate channel interferers, the dynamic range of the RF LNA and mixer can be greatly relaxed, allowing substantial power reductions. The absence of interferers also allows reductions in the phase noise requirements of the LO synthesizer required for down-conversion, providing further power savings.

To date, RF channel selection has been difficult to realize via present-day technologies. In particular, low-loss channel selection at RF would require tunable resonators with Q 's $> 10,000$ [5]. Unfortunately, such Q 's have not been available in the sizes needed for portable applications. In addition, high- Q often precludes tunability, making RF channel selection via a single RF filter a very difficult prospect. On the other hand, it is still possible to select individual RF channels via many non-tunable high- Q filters, one for each channel, and each switchable by command. Depending upon the communication standard, this could entail hundreds or thousands of filters—numbers that would be absurd if off-chip macroscopic filters are used, but that may be perfectly reasonable for microscale, passive, micromechanical filters. In the scheme of Fig. 17, a given filter (or set of them) is switched on (with all others

off) by decoder-controlled application of an appropriate dc-bias voltage to the desired filter. (From Section IV, a capacitively transduced resonator is on only when a finite dc-bias V_P is applied; i.e., with $V_P = 0$ V, the device is effectively an open circuit [29].)

The potential benefits afforded by this RF channel selector can be quantified by assessing its impact on the LNA linearity specification imposed by a given standard, e.g., the IS-98-A interim standard for code-division multiple-access (CDMA) cellular mobile stations [54]. In this standard, the required IIP_3 of the LNA is set mainly to avoid desensitization in the presence of a single tone (generated by the advanced mobile phone system (AMPS) [55]) spaced 900 kHz away from the CDMA signal center frequency. Here, reciprocal mixing of the local oscillator phase noise with the 900 kHz offset single tone and cross-modulation of the single tone with leaked transmitter power outputs dictate that the LNA IIP_3 exceeds +7.6 dBm [55]. However, if an RF channel select filter bank such as shown in Fig. 17 precedes the LNA and is able to reject the single tone by 40 dB, the requirement on the LNA then relaxes to $IIP_3 \leq -29.3$ dBm (assuming the phase noise specification of the local oscillator is *not* also relaxed). Given the well-known noise versus power trade-offs available in LNA design [56], such a relaxation in IIP_3 can result in nearly an order of magnitude reduction in power. In addition, since RF channel selection relaxes the overall receiver linearity requirements, it may become possible to put more gain in the LNA to suppress noise figure (NF) contributions from later stages, while relaxing the required NF of the LNA itself, leading to further power savings.

IX. PRACTICAL IMPLEMENTATION ISSUES

Of course, before anything as aggressive as an RF channel-selector can be realized, numerous practical implementation issues must still be overcome. Some of these issues were already described in Sections II and V, including aging and drift stability, temperature stability, motional impedance, and power handling (i.e., linearity). Although Sections II and V presented evidence that these issues were solvable, most of the demonstrated evidence was at frequencies below 100 MHz. While there is presently little reason to doubt they will come, demonstrations of adequate aging, drift, and temperature stability are still needed at GHz frequencies, as are demonstrations of antenna-amenable impedances past 1 GHz.

But beyond device-centric performance issues, there are a multitude of practical implementation issues that also must be overcome before vibrating RF MEMS technology can enter mainstream markets. Among the more important of these are absolute and matching fabrication tolerances, packaging, and (hybrid or fully integrated) merging with transistor circuits, all of which must be solved with the utmost in economy, given that cost is generally paramount in wireless markets.

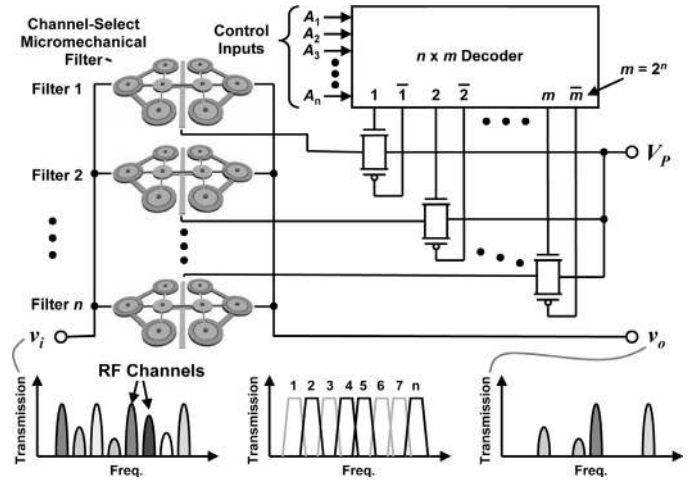


Fig. 17. Schematic diagram for an RF channel-select micromechanical filter bank, with an example showing how various input frequencies can be simultaneously selected via mere application or removal of resonator dc-biases. In the bottom plots, filters 2, 4, 5, and n are on, while all others are off.

A. Absolute and Matching Tolerances

Before embarking on this topic, it is worth mentioning that the advent of fractional- N synthesizers [57] now alleviates to some degree the accuracy requirements on high-volume reference oscillators for portable wireless devices. In particular, for many applications, the reference oscillator need no longer oscillate at an exactly trimmed frequency, but can rather oscillate at a frequency within a given range, as long as this frequency is stable against temperature and meets a minimum drift stability requirement. Obviously, this alleviates the minimum absolute fabrication tolerance required for a subset of high-volume frequency reference products, allowing their manufacture without the need for trimming, hence, without its added cost.

Of course, there are still many important present and future applications, such as timing and channel-select filtering, where absolute and matching tolerances are still of utmost importance. At the time of this writing, there are several companies endeavoring to commercialize vibrating RF MEMS technology, including Discera¹ and SiTime², both of which are pursuing timekeepers as initial products. Unfortunately, for obvious reasons, these companies do not publish manufacturing statistics. Thus, public data on yield and fabrication tolerances has so far been confined to publications by academia that most likely convey worst case numbers, given that university fabrication facilities are for research, not production.

Reference [58] presents one of the first published investigations on the absolute and matching tolerances of radial-mode disk resonators using polysilicon and polydiamond structural materials. From this preliminary work, the av-

¹Discera Micro Communication Technologies, San Jose, CA. <http://www.discera.com/>

²SiTime, <http://www.sitime.com/>

erage resonance frequency absolute and matching tolerances of 450 ppm and 343 ppm, respectively, measured for polysilicon disk resonators, are actually quite good. These values are, in fact, good enough to allow trimless implementation of 3% bandwidth RF pre-select or image-reject filters for wireless communications with a confidence interval better than 99.7% over tested dies that mismatch-induced passband distortion will be less than 0.3 dB [58]. In other words, all of the filters in the die of Fig. 8 could be wafer-level fabricated with the needed $\sim 3\%$ bandwidth filter specifications without any need for costly frequency trimming.

The fabrication tolerances of [58] are not, however, sufficient to realize the RF channel-select filter bank of Fig. 17 without trimming or some other mechanism to null offsets. In particular, since RF channel selection requires filters with percent bandwidths less than 0.2%, a resonator-to-resonator frequency matching tolerance better than 190 ppm would be needed if mismatch-induced passband ripple is to be held to less than 0.3 dB. Interestingly, as long as the matching tolerances are good, the absolute tolerance need not be so good for the bank of adjacent channel filters depicted in Fig. 17. This is because an absolute shift in frequency would shift the frequencies of all filters within a given standard's range by about the same amount. The filter responses would still be side-by-side in a bank covering the needed communication standard frequency range; just their center frequencies might be offset from their targeted positions by the same amount Δf . In this case, a simple global adjustment by $-\Delta f$, perhaps via a programmed shift in local oscillator frequency, would fix the frequency offset problem.

In the meantime, one should not rule out the possibility that a production wafer-level fabrication facility might actually be able to achieve matching tolerances on the order of 190 ppm, which would allow trimless (hence, low-cost) manufacturing of the RF channel selector of Fig. 17. If, in the end, such tolerances cannot be achieved, then perhaps methods for reducing matching tolerances by design can be applied. For example, mechanically coupled resonator arrays, such as used in rows 4–7 of Table III can actually average out variations in resonator frequency, lowering the overall matching tolerance between array-composite resonators.

If all else fails, laser trimming, such as described in [59], is still an option, although the cost of an LSI mechanical circuit like that of Fig. 17 would then become a function of the throughput of laser trimming.

B. Packaging

Packaging has historically been an impediment to commercialization of many MEMS-based products. Although cost has in general been the dominant reason, cost is less of an issue for vibrating RF MEMS devices, since a variety of low-cost wafer-level approaches to 0th level vacuum or hermetic packaging are already being used by companies commercializing MEMS-based timekeeper products. These

include packages based on wafer-level glass-frit bonding of caps [60] and low-pressure chemical vapor deposition (LPCVD) sealing of fully planar encapsulations [10], [61].

Aside from cost, an equally important package-related issue that greatly impacts the resonator-based timing and frequency control devices described here derives from the stresses induced by all levels of packaging, from device encapsulation (i.e., 0th level), to merging with transistors (i.e., 1st level), to board-level insertion (i.e., 2nd level). Such package stresses not only can shift the absolute center frequencies of micromechanical resonators, but also can often degrade their temperature sensitivity, induce hysteretic behavior in their frequency versus temperature curves, and cause undue frequency drift. Fortunately, the sheer geometric flexibility afforded by CAD-amenable micromechanical resonator design provides a wide palette of shapes and sizes with which to achieve a given frequency. This then allows a designer to defend against package stresses by selecting the geometry that best isolates the resonator from them. For example, a resonator anchored to the substrate at a single point, such as the disk resonator of row 4 in Table I, would be much more resilient against package stresses than the clamped-clamped beam of row 1, which is anchored to the substrate at two points, and so directly absorbs any package-derived substrate strains. Note that such an approach is not limited to just single resonators, as mechanically coupled resonator arrays supported at only one point can also be envisioned.

It is, however, more difficult to envision complete LSI mechanical circuits anchored at only one point. For these, other means for isolation from package stresses will need to be explored. Among possible solutions are: (1) implementation of the mechanical circuit on a platform that is itself isolated from the primary substrate; (2) the intermittent use of electrical coupling in places to keep the sizes of mechanical circuits small enough for single anchoring; or (3) the judicious use of very compliant mechanical couplers between major mechanical circuit chunks, wherever possible. Needless to say, the research already underway on methods for improved substrate isolation to maximize the Q of single resonators will likely continue, but this time with the aim of minimizing the package-stress susceptibility of mechanical circuits of such resonators.

C. Merging With Transistors

Often called the 1st level of packaging (where resonator encapsulation comprises the 0th level), merging with transistors via bonding, flip-chip bonding, or direct planar integration, might soon become the bottleneck to realization of the larger proposed mechanical circuits. In particular, the sheer number of leads needed from transistors to mechanics in the system of Fig. 17 favors a direct planar integration approach, such as that summarized in Figs. 2 and 3. To date, a more practical variant of the process of Fig. 2 using poly-SiGe structural material LPCVD-deposited at 450°C [15] has been demonstrated that should allow fully integrated merging of MEMS structures with

0.18- μm -channel-length CMOS using conventional metalization. However, merging with more advanced CMOS processes, e.g., with channel lengths 65 nm or lower, is still not available, since the very low- k dielectrics surrounding the metal interconnect in nm-CMOS processes generally demand a much lower post-transistor temperature ceiling than 450°C.

Thus, a new structural material that can be deposited at a very low temperature (e.g., less than the 320°C melting temperature of low- k Teflon dielectric), yet still retain very high Q at high frequency, is highly desirable. Recent literature suggests that nickel metal, which can be electroplated at 50°C, might be a strong candidate structural material. In particular, a nickel wine-glass disk resonator was recently demonstrated with a $Q > 50,000$ at 60 MHz [62], showing that nickel can indeed achieve Q 's on a par with polysilicon at VHF. Whether or not nickel's temperature dependence and aging behavior are also on a par with polysilicon is yet to be seen. Nevertheless, its VHF performance coupled with the low temperature of its deposition makes nickel a very intriguing prospect for modular post-transistor integration of vibrating RF MEMS with next generation nm-scale CMOS. Work in this vein is ongoing.

X. CONCLUSIONS

MEMS-based realizations of timing and frequency control functions, including 0.09% bandwidth filters with less than 0.6-dB insertion loss, GSM-compliant low phase noise oscillators, and miniature atomic clocks posting 5×10^{-11} at 100 s Allan deviation (so far) and consuming only 153 mW have been described with an emphasis on the performance benefits afforded by scaling to micro dimensions. In particular, via scaling, vibrating RF MEMS devices have now reached frequencies commensurate with critical RF functions in wireless applications and have done so with previously unavailable on-chip Q 's exceeding 10,000. Q 's this high may now encourage paradigm-shifting communication architectures that can eliminate interferers immediately after the antenna, allowing subsequent electronics to operate with much lower dynamic range and power consumption than would otherwise be needed. Given present transistor scaling trend towards lower dynamic range digital devices, such a relaxation in dynamic range requirements may be arriving at an opportune time.

At present, micromechanical circuit complexity is nearing medium-scale integration (MSI) density, as exemplified by the composite array filter in row 5 of Table III, which uses more than 43 resonators and links. Indeed, circuit complexity and frequency range should only increase as MEMS technologies evolve into NEMS (or "nanoelectromechanical system") technologies, with feature sizes that support frequencies exceeding 10 GHz. In fact, with knowledge of the micromechanical circuit concepts described herein, perhaps a reconsideration of the numerous ongoing research efforts to make transistors out of

nanowires is in order. In particular, one might ask: Is this the best way to use nanowires? After all, nanowires can be employed more naturally as vibrating resonators capable of doing mechanical signal processing when mechanically linked into circuit networks similar to those described herein. Such nanomechanical networks not only would be completely passive, consuming substantially less power, but also would dispense with the need for the electrical contacts that presently inhibit large-scale integration of nanowire transistors.

In the meantime, micromechanical resonator technology is making its way into commercial markets through several companies (e.g., Discera and SiTime) which are now sampling low-end timekeeper products based on this technology. Meanwhile, on the high-end front, the success of efforts to scale atomic clocks down to 10 cm³ (so far) strongly encourages ongoing efforts bent on shrinking them even further, down to 1-cm³ volume, while still posting 10⁻¹¹ Allan deviation at one hour with less than 30 mW of power consumption.

REFERENCES

- [1] A. A. Abidi, "Direct-conversion radio transceivers for digital comms," *IEEE J. Solid-State Circ.*, vol. 30, no. 12, pp. 1399–1410, Dec. 1995.
- [2] J. Crols and M. S. J. Steyaert, "A single-chip 900 MHz CMOS receiver front-end with a high performance low-IF topology," *IEEE J. Solid-State Circ.*, vol. 30, no. 12, pp. 1483–1492, Dec. 1995.
- [3] C. P. Yue and S. S. Wong, "On-chip spiral inductors with patterned ground shields for Si-based RF IC's," *IEEE J. Solid-State Circ.*, vol. 33, no. 5, pp. 743–752, May 1998.
- [4] C. T.-C. Nguyen, "Transceiver front-end architectures using vibrating micromechanical signal processors," in *RF Technologies for Low Power Wireless Communications*. G. I. Haddad, T. Itoh, and J. Harvey, Eds. New York: Wiley IEEE-Press, 2001, pp. 411–461.
- [5] C. T.-C. Nguyen, "Vibrating RF MEMS overview: applications to wireless communications (invited)," in *Proc. SPIE: Micromachin. Microfabric. Process Technol.*, San Jose, CA, vol. 5715, Jan. 22–27, 2005, pp. 11–25.
- [6] J. Wang, J. E. Butler, T. Feygelson, and C. T.-C. Nguyen, "1.51-GHz polydiamond micromechanical disk resonator with impedance-mismatched isolating support," in *Proc. IEEE Int. MEMS Conf.*, Maastricht, The Netherlands, Jan. 25–29, 2004, pp. 641–644.
- [7] S.-S. Li, Y.-W. Lin, Y. Xie, Z. Ren, and C. T.-C. Nguyen, "Micromechanical hollow-disk ring resonators," in *Proc. 17th IEEE Int. MEMS Conf.*, Maastricht, The Netherlands, Jan. 25–29, 2004, pp. 821–824.
- [8] W.-T. Hsu and C. T.-C. Nguyen, "Stiffness-compensated temperature-insensitive micromechanical resonators," in *Tech. Dig., IEEE Int. MEMS Conf.*, Las Vegas, NV, Jan. 20–24, 2002, pp. 731–734.
- [9] V. Kaajakari, J. Kiihamäki, A. Oja, H. Seppä, S. Pietikäinen, V. Kokkala, and H. Kuisma, "Stability of wafer level vacuum encapsulated single-crystal silicon resonators," in *Tech. Dig., Int. Conf. Solid-State Sensors, Actuators, Microsyst. (Transducers'05)*, Seoul, Korea, Jun. 2005, pp. 916–919.
- [10] B. Kim, R. N. Candler, M. Hopcroft, M. Agarwal, W.-T. Park, and T. W. Kenny, "Frequency stability of wafer-scale encapsulated MEMS resonators," in *Tech. Dig., Int. Conf. Solid-State Sensors, Actuators, Microsyst. (Transducers'05)*, Seoul, Korea, Jun. 2005, pp. 1965–1968.
- [11] Y.-W. Lin, S.-S. Li, Z. Ren, and C. T.-C. Nguyen, "Low phase noise array-composite micromechanical wine-glass disk oscillator," in *Tech. Dig., IEEE Int. Electron Devices Mtg.*, Washington, DC, Dec. 5–7, 2005, pp. 287–290.

- [12] Y.-W. Lin, S. Lee, S.-S. Li, Y. Xie, Z. Ren, and C. T.-C. Nguyen, "Series-resonant VHF micromechanical resonator reference oscillators," *IEEE J. Solid-State Circ.*, vol. 39, no. 12, pp. 2477–2491, Dec. 2004.
- [13] V. Kaajakari, T. Mattila, A. Oja, J. Kiihamäki, and H. Seppä, "Square-extensional mode single-crystal silicon micromechanical resonator for low-phase-noise oscillator applications," *IEEE Electron Device Lett.*, vol. 25, no. 4, pp. 173–175, Apr. 2004.
- [14] C. T.-C. Nguyen and R. T. Howe, "An integrated CMOS micromechanical resonator high- Q oscillator," *IEEE J. Solid-State Circ.*, vol. 34, no. 4, pp. 440–455, Apr. 1999.
- [15] A. E. Franke, J. M. Heck, T.-J. King, and R. T. Howe, "Polycrystalline silicon-germanium films for integrated microsystems," *IEEE/ASME J. Microelectromech. Syst.*, vol. 12, no. 2, pp. 160–171, Apr. 2003.
- [16] T. A. Core, W. K. Tsang, and S. J. Sherman, "Fabrication technology for an integrated surface-micromachined sensor," *Solid State Technol.*, pp. 39–47, Oct. 1993.
- [17] R. C. Ruby, P. Bradley, Y. Oshmyansky, A. Chien, and J. D. Larson, III, "Thin film bulk wave acoustic resonators (FBAR) for wireless applications," in *Proc. IEEE Ultrason. Symp.*, Atlanta, GA, 2001, pp. 813–821.
- [18] H. Yu, W. Pang, H. Zhang, and E. S. Kim, "Film bulk acoustic resonator at 4.4 GHz with ultra low temperature coefficient of resonant frequency," in *Tech. Dig., 18th IEEE Int. MEMS Conf.*, Miami Beach, FL, Jan. 30–Feb. 3, 2005, pp. 28–31.
- [19] F. D. Bannon, III, J. R. Clark, and C. T.-C. Nguyen, "High frequency micromechanical filters," *IEEE J. Solid-State Circ.*, vol. 35, no. 4, pp. 512–526, Apr. 2000.
- [20] K. Wang, A.-C. Wong, and C. T.-C. Nguyen, "VHF free-free beam high- Q micromechanical resonators," *IEEE/ASME J. Microelectromech. Syst.*, vol. 9, no. 3, pp. 347–360, Sep. 2000.
- [21] M. A. Abdelmoneum, M. U. Demirci, and C. T.-C. Nguyen, "Stemless wine-glass-mode disk micromechanical resonators," in *Proc. 16th IEEE Int. MEMS Conf.*, Kyoto, Japan, Jan. 19–23, 2003, pp. 698–701.
- [22] J. Wang, Z. Ren, and C. T.-C. Nguyen, "1.156-GHz self-aligned vibrating micromechanical disk resonator," *IEEE Trans. Ultrason., Ferroelect., Freq. Contr.*, vol. 51, no. 12, pp. 1607–1628, Dec. 2004.
- [23] M. U. Demirci and C. T.-C. Nguyen, "Higher-mode free-free beam micromechanical resonators," in *Proc. IEEE Int. Freq. Contr. Symp.*, Tampa, FL, May 5–8, 2003, pp. 810–818.
- [24] X. M. H. Huang, C. A. Zorman, M. Mehregany, and M. L. Roukes, "Nanodevice motion at microwave frequencies," *Nature*, vol. 421, p. 496, Jan. 30, 2003.
- [25] J. R. Vig and Y. Kim, "Noise in microelectromechanical system resonators," *IEEE Trans. Ultrason., Ferroelect., Freq. Contr.*, vol. 46, no. 6, pp. 1558–1565, Nov. 1999.
- [26] B. Bircumshaw, G. Lui, H. Takeuchi, T.-J. King, R. T. Howe, O. O'Reilly, and A. P. Pisano, "The radial bulk annular resonator: Towards a 50 Ω MEMS filter," in *Tech. Dig., Transducers'03*, Boston, MA, Jun. 8–12, 2003, pp. 875–878.
- [27] Y. Xie, S.-S. Li, Y.-W. Lin, Z. Ren, and C. T.-C. Nguyen, "UHF micromechanical extensional wine-glass mode ring resonators," in *Tech. Dig., IEEE Int. Electron Devices Mtg.*, Washington, DC, Dec. 8–10, 2003, pp. 953–956.
- [28] A.-C. Wong and C. T.-C. Nguyen, "Micromechanical mixer-filters ("mixlers")," *IEEE/ASME J. Microelectromech. Syst.*, vol. 13, no. 1, pp. 100–112, Feb. 2004.
- [29] S.-S. Li, Y.-W. Lin, Z. Ren, and C. T.-C. Nguyen, "Self-switching vibrating micromechanical filter bank," in *Proc. IEEE Joint Int. Freq. Contr./Precision Time & Time Interval Symp.*, Vancouver, Canada, Aug. 29–31, 2005, pp. 135–141.
- [30] H. Nathanson, W. E. Newell, R. A. Wickstrom, and J. R. Davis, Jr., "The resonant gate transistor," *IEEE Trans. Electron Devices*, vol. ED-14, no. 3, pp. 117–133, Mar. 1967.
- [31] S. Pourkamali, Z. Hao, and F. Ayazi, "VHF single crystal silicon capacitive elliptic bulk-mode disk resonators—Part II: Implementation and characterization," *IEEE/ASME J. Microelectromech. Syst.*, vol. 13, no. 6, pp. 1054–1062, Dec. 2004.
- [32] S. Pourkamali, G. K. Ho, and F. Ayazi, "Vertical capacitive SiBARs," in *Tech. Dig., 18th IEEE Int. MEMS Conf.*, Miami Beach, FL, Jan. 30–Feb. 3, 2005, pp. 211–214.
- [33] G. Piazza, P. J. Stephanou, J. M. Porter, M. B. J. Wijesundara, and A. P. Pisano, "Low motional resistance ring-shaped contour-mode aluminum nitride piezoelectric micromechanical resonators for UHF applications," in *Tech. Dig., 18th IEEE Int. MEMS Conf.*, Miami Beach, FL, Jan. 30–Feb. 3, 2005, pp. 20–23.
- [34] F. P. Stratton, D. T. Chang, D. J. Kirby, R. J. Joyce, T.-Y. Hsu, R. L. Kubena, and Y.-K. Yong, "A MEMS-based quartz resonator technology for GHz applications," in *Proc. IEEE Int. Ultrason., Ferroelect., Freq. Contr. Conf.*, Montreal, Canada, Aug. 24–27, 2004, pp. 27–34.
- [35] Y.-W. Lin, S.-S. Li, Z. Ren, and C. T.-C. Nguyen, "Vibrating micromechanical resonators with solid dielectric capacitive-transducer 'gaps'," in *Proc. Joint IEEE Int. Freq. Contr./Precision Time & Time Interval Symp.*, Vancouver, Canada, Aug. 29–31, 2005, pp. 128–134.
- [36] D. Weinstein, H. Chandrahilim, L. F. Cheow, and S. A. Bhavé, "Dielectrically transduced single-ended to differential MEMS filter," in *Tech. Dig., IEEE Int. Solid-State Circuits Conf.*, San Francisco, CA, Feb. 5–9, 2006, pp. 318–319.
- [37] K. Wang and C. T.-C. Nguyen, "High-order medium frequency micromechanical electronic filters," *IEEE/ASME J. Microelectromech. Syst.*, vol. 8, no. 4, pp. 534–557, Dec. 1999.
- [38] S.-S. Li, M. U. Demirci, Y.-W. Lin, Z. Ren, and C. T.-C. Nguyen, "Bridged micromechanical filters," in *Proc. IEEE Int. Ultrason., Ferroelect., Freq. Contr. Conf.*, Montreal, Canada, Aug. 24–27, 2004, pp. 144–150.
- [39] M. Demirci and C. T.-C. Nguyen, "Mechanically corner-coupled square microresonator array for reduced series motional resistance," *IEEE/ASME J. Microelectromech. Syst.*, vol. 15, no. 6, pp. 1419–1436, Dec. 2006.
- [40] M. U. Demirci and C. T.-C. Nguyen, "A low impedance VHF micromechanical filter using coupled-array composite resonators," in *Tech. Dig., 13th Int. Conf. Solid-State Sensors & Actuators (Transducers'05)*, Seoul, Korea, Jun. 5–9, 2005, pp. 2131–2134.
- [41] S.-S. Li, Y.-W. Lin, Z. Ren, and C. T.-C. Nguyen, "Disk-array design for suppression of unwanted modes in micromechanical composite-array filters," in *Tech. Dig., 19th IEEE Int. MEMS Conf.*, Istanbul, Turkey, Jan. 22–26, 2006, pp. 866–869.
- [42] R. Navid, J. R. Clark, M. Demirci, and C. T.-C. Nguyen, "Third-order intermodulation distortion in capacitively-driven CC-beam micromechanical resonators," in *Tech. Dig., 14th IEEE Int. MEMS Conf.*, Interlaken, Switzerland, Jan. 21–25, 2001, pp. 228–231.
- [43] A. T. Alastalo and V. Kaajakari, "Intermodulation in capacitively coupled microelectromechanical filters," *IEEE Electron Device Lett.*, vol. 26, no. 5, pp. 289–291, May 2005.
- [44] Y.-W. Lin, S.-S. Li, Z. Ren, and C. T.-C. Nguyen, "Third-order intermodulation distortion in capacitively-driven VHF micromechanical resonators," in *Proc. IEEE Ultrason. Symp.*, Sep. 18–21, 2005, pp. 1592–1595.
- [45] D. B. Leeson, "A simple model of feedback oscillator noise spectrum," *Proc. IEEE*, vol. 54, pp. 329–330, Feb. 1966.
- [46] M. Tiebout, "Low-power low-phase-noise differentially tuned quadrature VCO design in standard CMOS," *IEEE J. Solid-State Circ.*, vol. 36, no. 7, pp. 1018–1024, Jul. 2001.
- [47] Data sheet, Model CVHD-950, ultra-low phase noise voltage controlled crystal oscillator, Ft. Myers, FL: Crystek Crystals Corp..
- [48] S. Lee and C. T.-C. Nguyen, "Mechanically-coupled micromechanical arrays for improved phase noise," in *Proc. IEEE Int. Ultrason., Ferroelect., Freq. Contr. Conf.*, Montreal, Canada, Aug. 24–27, 2004, pp. 280–286.
- [49] S. Lee and C. T.-C. Nguyen, "Influence of automatic level control on micromechanical resonator oscillator phase noise," in *Proc. IEEE Int. Freq. Contr. Symp.*, Tampa, FL, May 5–8, 2003, pp. 341–349.
- [50] V. Kaajakari, J. K. Koskinen, and T. Mattila, "Phase noise in capacitively coupled micromechanical oscillators," *IEEE Trans. Ultrason., Ferroelect., Freq. Contr.*, vol. 52, no. 12, pp. 2322–2331, Dec. 2005.
- [51] C. T.-C. Nguyen and R. T. Howe, "Microresonator frequency control and stabilization using an integrated micro oven," in *Tech. Dig., 7th Int. Conf. Solid-State Sensors Actuators (Transducers'93)*, Yokohama, Japan, Jun. 7–10, 1993, pp. 1040–1043.
- [52] R. Lutwak, J. Deng, W. Riley, M. Varghese, J. Leblanc, G. Tepolt, M. Mescher, K. K. Serkland, K. M. Geib, and G. M. Peake, "The chip-scale atomic clock—low-power physics package," in *Proc. Precision Time and Time Interval (PTTI) Syst. Applic. Mtg.*, Washington, DC, Dec. 7–9, 2004.

- [53] L. Liew, S. Knappe, J. Moreland, H. G. Robinson, L. Hollberg, and J. Kitching, "Microfabricated alkali atom vapor cells," *Appl. Phys. Lett.*, vol. 84, pp. 2694–2696, Apr. 2004.
- [54] *Recommended Minimum Performance Standards for Dual-mode Wideband Spread Spectrum Cellular Mobile Stations, TIA/EIA/IS-98-A Interim Standard*, Jul. 1996.
- [55] W. Y. Ali-Ahmad, "RF system issues related to CDMA receiver specifications," *RF Design*, pp. 22–32, Sep. 1999.
- [56] D. K. Shaeffer and T. H. Lee, "A 1.5-V, 1.5-GHz CMOS low noise amplifier," *IEEE J. Solid-State Circ.*, vol. 32, no. 5, pp. 745–759, May 1997.
- [57] B. G. Goldberg, "The evolution and maturity of fractional-N PLL synthesizers," *Microwave J.*, pp. 124–134, Sep. 1996.
- [58] J. Wang, Y. Xie, and C. T.-C. Nguyen, "Frequency tolerance of RF micromechanical disk resonators in nanocrystalline diamond and polysilicon structural materials," in *Tech. Dig., IEEE Int. Electron Devices Mtg.*, Washington, DC, Dec. 5–7, 2005, pp. 291–294.
- [59] M. A. Abdelmoneum, M. U. Demirci, Y.-W. Lin, and C. T.-C. Nguyen, "Location-dependent tuning of vibrating micromechanical resonators via laser trimming," in *Proc. IEEE Int. Ultrason., Ferroelect., Freq. Contr. Conf.*, Montreal, Canada, Aug. 24–27, 2004, pp. 272–279.
- [60] D. Sparks, S. Massoud-Ansari, and N. Najafi, "Long-term evaluation of hermetically glass frit sealed silicon to Pyrex wafers with feedthroughs," *J. Micromech. Microeng.*, vol. 15, pp. 1560–1564, 2005.
- [61] K. S. Leboutz, A. Mazaheri, R. T. Howe, and A. P. Pisano, "Vacuum encapsulation of resonant devices using permeable polysilicon," in *Tech. Dig., 12th IEEE Int. MEMS Conf.*, Orlando, FL, Jan. 17–21, 1999, pp. 470–475.
- [62] W.-L. Huang, Z. Ren, and C. T.-C. Nguyen, "Nickel vibrating micromechanical disk resonator with solid dielectric capacitive-transducer gap," in *Proc. IEEE Int. Freq. Contr. Symp.*, Miami, FL, Jun. 5–7, 2006, pp. 839–847.



Clark T.-C. Nguyen (S'90–M'95–SM'01–F'07) received the B.S., M.S., and Ph.D. degrees from the University of California at Berkeley in 1989, 1991, and 1994, respectively, all in electrical engineering and computer sciences.

In 1995, he joined the faculty of the University of Michigan, Ann Arbor, where he was a professor in the Department of Electrical Engineering and Computer Science until mid-2006. In 2006, he joined the faculty of the University of California at Berkeley, where he is presently a professor in the Department of Electrical Engineering and Computer Sciences. His research interests focus upon microelectromechanical systems (MEMS) and include integrated micromechanical signal processors and sensors, merged circuit/micromechanical technologies, RF communication architectures, and integrated circuit design and technology. From 1995 to 1997, he was a member of the National Aeronautics and Space Administration (NASA)'s New Millennium Integrated Product Development Team on Communications, which roadmapped future communications technologies for NASA use into the turn of the century. In 2001, Prof. Nguyen founded Discera, Inc., a company aimed at commercializing communication products based upon MEMS technology, with an initial focus on the very vibrating micromechanical resonators pioneered by his research in past years. He served as Vice President and Chief Technology Officer (CTO) of Discera until mid-2002, at which point he joined the Defense Advanced Research Projects Agency (DARPA) on an IPA, where he served for 3.5 years as the Program Manager of the MEMS, Micro Power Generation (MPG), Chip-Scale Atomic Clock (CSAC), MEMS Exchange (MX), Harsh Environment Robust Micromechanical Technology (HERMIT), Micro Gas Analyzers (MGA), Radio Isotope Micropower Sources (RIMS), RF MEMS Improvement (RFMIP), Navigation-Grade Integrated Micro Gyroscopes (NGIMG), and Micro Cryogenic Coolers (MCC) programs, in the Microsystems Technology Office of DARPA.

Prof. Nguyen received the 1938E Award for Research and Teaching Excellence from the University of Michigan in 1998, an EECS Departmental Achievement Award in 1999, the Ruth and Joel Spira Award for Teaching Excellence in 2000, the University of Michigan's 2001 Henry Russel Award, and the Cady Award from the 2006 IEEE Frequency Control Symposium. Among his publication accolades are the Jack Raper Award from 2005 IEEE International Solid-State Circuits Conference, the 2004 DARPA Tech Best Technical Presentation Award, the Best Invited Paper Award at the 2004 IEEE Custom Integrated Circuits Conference, and, together with his students, the Best Student Paper Award in Category 1 at the 2005 Joint IEEE Frequency Control/Precise Time and Timing Interval (PTTI) Symposium, the Best Student Paper Award in the Frequency Control Category at the 2004 IEEE Ultrasonics, Ferroelectrics, and Frequency Control Symposium, and the Roger A. Haken Best Student Paper Awards at the 1998 and 2003 IEEE International Electron Devices Meetings. To date, he has organized and chaired a total of 35 IEEE and DARPA workshops.